Glaciolacustrine deposits formed in an ice-dammed tributary valley in the south-central Pyrenees: new evidence for late Pleistocene climate

Carlos Sancho[1], Concha Arenas[1*], Gonzalo Pardo[1], José Luis Peña-Monné[2], Edward J. Rhodes[3], Miguel Bartolomé[4], José M. García-Ruiz[4], Carlos Martí-Bono[4]

[1] Departamento de Ciencias de la Tierra, Universidad de Zaragoza, Pedro Cerbuna 12, 50009 Zaragoza, Spain

[2] Departamento de Geografía y Ordenación del Territorio, Universidad de Zaragoza, Pedro Cerbuna 12, 50009 Zaragoza, Spain

[3] Department of Geography, The University of Sheffield, Sheffield S10 2TN, UK

[4] Instituto Pirenaico de Ecología, Consejo Superior de Investigaciones Científicas (IPE-CSIC), Apartado 13.034, 50080 Zaragoza, Spain

* Corresponding author

Abstract

Combined geomorphic features, stratigraphic characteristics and sedimentologic interpretation, coupled with optically stimulated luminescence (OSL) dates, of a glacio-fluvio-lacustrine sequence (Linás de Broto, northern Spain) provide new information to understand the palaeoenvironmental significance of dynamics of glacier systems in the

south-central Pyrenees during the Last Glacial Cycle (≈ 130 ka to 14 ka). The Linás de Broto depositional system consisted of a proglacial lake fed primarily by meltwater streams emanating from the small Sorrosal glacier and dammed by a lateral moraine of the Ara trunk glacier. The resulting glacio-fluvio-lacustrine sequence, around 55 m thick, is divided into five lithological units consisting of braided fluvial (gravel deposits), lake margin (gravel and sand deltaic deposits) and distal lake (silt and clay laminites) facies associations. Evolution of the depositional environment reflects three phases of progradation of a high-energy braided fluvial system separated by two phases of rapid expansion of the lake. Fluvial progradation occurred during short periods of ice melting. Lake expansion concurred with ice-dam growth of the trunk glacier. The first lake expansion occurred over a time range between 55±9 ka and 49±11 ka, and is consistent with the age of the Viu lateral moraine (49±8 ka), which marks the maximum areal extent of the Ara glacier during the Last Glacial Cycle. These dates confirm that the maximum areal extent of the glacier occurred during Marine Isotope Stages 4 and 3 in the south-central Pyrenees, thus before the Last Glacial Maximum. The evolution of the Linás de Broto depositional system during this maximum glacier extent was modulated by climate oscillations in the northern Iberian Peninsula, probably related to latitudinal shifts of the atmospheric circulation in the southern North-Atlantic Ocean, and variations in summer insolation intensity.

Key words: glaciolacustrine sediments; ice-dammed lake; maximum glacier extent; Marine Isotope Stages 4 and 3; south-central Pyrenees.

1. Introduction

The south Pyrenean Quaternary glaciations have been the subject of study since the 19th century (see compilation by Chueca et al., 1998). Regional mapping and detailed geomorphology (Vilaplana, 1983; Bordonau, 1992; Martí-Bono, 1996; Serrano, 1998), and indirect dates from lacustrine records allowed refining the reconstruction of the glacial evolution (Montserrat-Martí, 1992; García-Ruiz et al., 2003; González-Sampériz et al., 2006). The asynchronous character of the maximum glacier advances in the south-central Pyrenees during the Last Glacial Cycle (LGC) relative to the Last Glacial Maximum (LGM) was then postulated. The LGC is defined as the last cold stage between Termination II (130 ka) and Termination I (14 ka) (Gibbard and Cohen, 2008; Hughes et al., 2013). Dating of glacial records based on optically stimulated luminescence (OSL) (Sancho et al., 2003; Lewis et al., 2009; García-Ruiz et al., 2013) and terrestrial cosmogenic nuclides (TCN) (Delmas et al., 2008; Pallás et al., 2010; Calvet et al., 2011) confirmed such a hypothesis. Dating the maximum ice extent through the Mediterranean realm during the LGC (e.g., Hughes et al., 2006a, b, 2013; Hughes and Woodward, 2008) is a matter of debate during the last decade in other mountains in the Iberian Peninsula (e.g., Palacios et al., 2011; Jiménez-Sánchez et al., 2013; Dominguez-Villar et al., 2013; Carrasco et al., 2015; Rodríguez-Rodríguez et al., 2016).

Glaciolacustrine environments are exceptionally sensitive to environmental changes and climate oscillations at different time scales (e.g., Matthews et al., 2000; Gruszka, 2001; Johnsen and Brennand, 2006; Shulmeister et al., 2010; Turu et al., 2017; Smith, 2017). The southern Pyrenean glacial records include glaciolacustrine deposits, e.g., in

66 the River Aragón Subordán valley (La Reclusa) (Martí-Bono, 1977), the River Gállego
67 valley (Aso de Sobremonte) (Serrano, 1998), the River Esera valley (Cerler) (Bordonau,
68 1992), the River Noguera Ribagorzana valley (Llauset and Llestui) (Serrat et al., 1982;
69 Vilaplana et al., 1983, 1989; Monserrat and Vilaplana, 1988; Bordonau et al., 1993) and
70 the River Valira valley (La Massana) (Serrat et al., 1982; Turu, 2002; Turu et al., 2017).
71 Among these, the glaciolacustrine sequence of Linás de Broto, formed in relation to
72 ice-damming by the River Ara valley (Huesca Province), constitutes a classical record in
73 the south-central Pyrenees, known since the late 19th century (Mallada, 1878; Penck,
74 1883; Serrat et al., 1982; Martí-Bono and García-Ruiz, 1994; Martí-Bono, 1996; Martí-
75 Bono et al., 2002).

76 Although previous work on the glacio-fluvio-lacustrine record of Linás de Broto has
77 dealt with geomorphology (Martí-Bono, 1996), sedimentology (Serrat et al., 1982) and
78 chronology (Martí-Bono et al., 2002; Sancho et al., 2011), conclusive results in regard
79 to timing and depositional evolution of such record in relation to climatic parameters
80 and other glacial records are still missing. As a consequence, this work aims to i) define
81 precisely the depositional evolution of this glacio-fluvio-lacustrine sequence with
82 respect to the relevant sedimentary processes and climatic conditions, and ii) place
83 this record chronologically within the evolution of the south Pyrenean glaciation
84 during the LGC. For this purpose, new geomorphologic, sedimentologic and
85 chronologic (based on OSL) data of the Linás de Broto sequence have been obtained.

86 **2. Study area**

In the south-central Pyrenees (northern Spain) (Fig. 1A), the Quaternary glaciofluvial and glaciolacustrine deposits of Linás de Broto, which are the focus of this work, fill the lower reach of the River Sorrosal valley, a tributary of the River Ara valley (Fig. 2A).

From a geological point of view (Fig. 1B), the study area is located in the south Pyrenean thrust-and-fold belt (Muñoz, 2002). The outcropping bedrock in the River Sorrosal watershed is composed of Upper Cretaceous-Paleocene limestones, dolostones and sandstones of the Internal Sierras, and Eocene turbidites of the Jaca Basin (Barnolas and Pujalte, 2004) (Fig. 2A). These materials show a complex structure with tight folds and imbricated thrust sheets (Ríos et al., 1982).

Present climate in the Sorrosal valley bottom is cool temperate (Oceanic-Mediterranean transition), with a mean annual temperature of 8.5-9.0 °C and a mean annual precipitation of around 850 mm (López et al., 2007). However, colder conditions (around 0°C of average annual temperature, following estimations from Del Barrio et al., 1990) with high snowfall (more than 2000 mm of annual precipitation, as deduced from De la Riva, 2000) dominate the highest areas of the watershed (up to 2845 m).

The present landscape of the River Sorrosal watershed, with an area of 42 km^2, is related to fluvial incision and glacial activity persisting throughout the Quaternary on the deformed Mesozoic-Cenozoic bedrock. Pleistocene deposition is represented by moraines, glaciolacustrine deposits and staircase fluvial terraces (Martí-Bono, 1996) (Fig. 2A). A sharp escarpment related to three small coalescent glacial cirques, formed within folded Upper Cretaceous-Paleocene rocks, occurs in the northern sector of the

River Sorrosal watershed. The upper sector of the valley presents U-shaped morphology, and moraine remnants corresponding to three stages of glacier stabilization can be recognized (S1, S2 and S3 in Fig. 2A). Slope and periglacial morphologies (rock glaciers) complete the landscape of the uppermost sector of the River Sorrosal valley (Fig. 2A).

A moraine formed of two very close ridges, separated by a paleovalley, can be distinguished near the village of Viu (A1.a and A1.b in Fig. 2B). It was deposited as a lateral moraine during the maximum extent of the Ara glacier, an ice tongue around 32 km in length flowing from the Vignemale massif (3299 m a.s.l.), when it was approximately 400 m thick at that sector and terminated near the Asín de Broto village (800 m a.s.l.), approximately 8.5 km down-valley from the Viu morraine (Serrano and Martínez de Pisón, 1994; Martí Bono et al., 2002) (Fig. 2C). A sedimentary unit made of gravels and sands, probably related to a kame terrace deposited against till deposits, has been recognized on the southwestern side of the Viu moraine (Martí-Bono, 1996) (A1.c in Fig. 2B). Sand lenses in this kame terrace deposits were sampled for OSL dating (Sancho et al., 2011).

At present, the morphogenetic surface associated with the fluviolacustrine deposits (Q1 terrace in Fig. 2A, B) is 60 m above the present river channel. The deposits of terrace Q1 comprise fluvial and lacustrine facies. The geomorphic relationship between the external lateral moraine of the Ara glacier (i.e., Viu moraine; A1 in Fig. 2B) and the glaciolacustrine record to the west-northwest (e.g., locus of measured sections LB1 and LB2, Fig. 2B) in the Pleistocene is very clear, taking into account the relative spatial position and elevation of the top of the glaciolacustrine deposits and the

external moraine. Upstream of Linás de Broto (north of the village), the Q1 terrace of the River Sorrosal has been identified forming an elongated (2.7 km) and very narrow bench on the east side of the valley (Fig. 2A).

Another lateral moraine of the Ara glacier is located close to the village of Fragen (A2 in Fig. 2B); its more internal position respect to the Viu moraine (A1 in Fig. 2B) indicates a later retreat stage of the glacier. The occurrence of a small lake related to that lateral moraine in Fragen is not rejected, but any related lacustrine deposits have not been recognised in the field. This younger aggradational glacier stage may explain the middle staircase terrace identified along the River Sorrosal at Linás de Broto and other upstream sites on the right side of the valley (Q2 terrace in Fig. 2A, B). Finally, a lower staircase terrace related to the River Sorrosal has been identified around the village of Linás de Broto (Q3 terrace in Fig. 2A, B).

In brief, in Pleistocene times at least two stages (Viu and Fragen glacial phases) of the Ara glacier stabilization can be deduced from preserved lateral moraines at Viu and Fragen (A1 and A2 in Fig. 2A, B). The Viu phase represents the maximum ice advance of the Ara glacier during the LGC (Serrano and Martínez de Pisón, 1994; Martí-Bono, 1996). The Sorrosal glacier did not join the Ara glacier, and a proglacial lake separated these two glaciers. The deposits of such a lake (represented in terrace Q1) are studied in this paper.

3. Methods

An aerial photographic base (Interministerial flight 1978, scale 1:18,000; Aragón flight 2006, scale 1:30,000) and Google Earth images from 2016 were used for mapping of

154 the River Sorrosal catchment. Extensive field investigations and mapping were
155 undertaken to confirm the presence and nature of mapped moraines, lacustrine
156 deposits and terraces. At a natural scarp formed by the incision of the River Sorrosal
157 close to the villages of Linás de Broto and Viu, two stratigraphic-sedimentologic
158 sections were measured through the Quaternary deposits (LB1 and LB2; Figs. 2B, 3).
159 The outcrops were logged and correlations between the stratigraphic sections made
160 using a composite panoramic photographic image (Figs. 3, 4A). Sedimentary facies
161 were characterized on the basis of lithology, bed geometry, texture and sedimentary
162 structures. The sedimentary lithofacies codes of Miall (1978) were used in
163 sedimentologic analysis (Table 1), and lithofacies associations were established.
164 Laminated facies were studied for textural and structural characterization with thin
165 sections (from eight samples) using a petrographic microscope. Scanning electron
166 microscopy (SEM) was applied to help mineral identification using X-ray elemental
167 microanalyses (Carl Zeiss MERLIN^{TM}, Carl Zeiss Group, Jena, Germany) in the case of
168 four fine-grained samples, operating at 3-5 kV and 150-500 pA. Powder from four fine-
169 grained samples was used to establish the mineralogical composition by X-Ray
170 Diffraction, using a D-Max Rigaku diffractometer equipped with a graphite
171 monochromator and CuKa radiation. XRD and SEM determinations were made at the
172 *Servicios de Apoyo a la Investigación* (SAI) of the University of Zaragoza (Spain).

173 Optically stimulated luminescence (OSL) dating was undertaken using well-sorted
174 sandy deposits from section LB1 (Fig. 3), and preliminary results were first presented
175 by Sancho et al. (2011), although methods were not explained or the implications
176 discussed in that summary. The OSL analyses of four samples (Table 2) were performed

177 at the Luminescence Dating Laboratory of the Research Laboratory for Archaeology
178 and the History of Art (University of Oxford, UK). Quartz grains within the size range of
179 125-250 μm were extracted as described by Rhodes (1988). Sample preparation
180 included sieving, etching with concentrated hydrofluoric acid (HF), and sodium
181 polytungstate density separation of heavy minerals. A single aliquot regenerative-dose
182 (SAR) protocol (Murray and Wintle, 2000, 2003) was used for OSL dating, with
183 measurements made on a Risø TL-DA-15 automated luminescence reader. In-situ
184 gamma ray spectrometry (Rhodes and Schwenninger, 2007) was used to estimate the
185 environmental dose rate. Using values derived from measured water content samples,
186 a value of 15±5% was applied in the age calculations.

187 ***4. Stratigraphy and sedimentology***

188 4.1 Stratigraphic sections

189 Two stratigraphic sections were measured to the southeast of Linás de Broto (location
190 in Fig. 2B). These sections –LB1 and LB2– are 56 and 53 m thick, respectively (Fig. 3).
191 The lowest part of the outcropping succession can be observed on a scarp excavated
192 by lateral erosion of the present River Sorrosal between these sections. That part
193 consists of ≈ 2.5 m thick alternating gravel and sand beds (Figs. 3, 4B).

194 In these sections eighteen sedimentary facies were identified based on lithology, bed
195 geometry, texture and sedimentary structures. Their main textural and structural
196 features, and their depositional interpretation are summarized in Table 1 and are
197 illustrated in Figures 4 to 9.

198 Gravels are present along the two sections (Fig. 3). Many parts of them are
199 structureless (facies Gm), occasionally with clast imbrication, though horizontal
200 stratification and trough and planar cross-stratification (facies Gh, Gt and Gp) are
201 present (Fig. 5A-F).

202 Sands form centimetre- to decimetre-thick, tabular and less common lenticular bodies
203 that can be structureless (Sm), but commonly show horizontal lamination (Sh), ripple
204 lamination and ripples (Sr) (Fig. 6). Flame structures and contorted lamination are
205 conspicuous features of these facies (Fig. 9). Lense- and sigmoid-shaped coarse-sand
206 bodies, decimetre-thick, form foreset cross-stratification (Sf). In some cases, facies Sf
207 associate laterally and vertically to facies Gf and Gm, e.g., at the base of the studied
208 sequence (Figs. 4B, 5F-H).

209 Silts and clays are more abundant in section LB2, being either structureless (Fm and
210 Clm) or with horizontal and ripple lamination (Fh, Clh and Fr) (Figs. 7, 8). Dropstones
211 (mm to ≈ 1 m long) are common in the clay layers. In some areas, beds formed of
212 sands and silts, and minor gravels, show metre-scale folds (Fig. 9A, B).

213 Five lithological units were differentiated and correlated based on the physical
214 continuity of several gravel bodies throughout the outcropping deposit (Figs. 3, 4A).

215 Unit 1 is 12 m thick in LB1 and 8.3 m thick in LB2. It is mostly formed of clast-supported
216 gravels with minor sands and occasional mud intercalations. With respect to grain size,
217 maximum values varies between 19 and 32 cm in LB1 and between 15 and 22 cm in
218 LB2. Single larger clasts, 0.5 to 1.2 m long, appear in the upper third of the unit. These
219 coarse facies form tabular bodies, up to 3 m thick, with irregular and erosive bases,

and may show gentle concave internal surfaces. Most common facies in Unit 1 are Gm and Gh, along with Gt and Gp that are associated with St and Sp (see Table 1 for facies codes). Fining upward deposits, up to 0.6 m thick, made of Gh and Sh are more common in section LB2. Sands may also constitute lenticular bodies, cm to 0.2 m thick, either as Sm, Sh or St. Lenticular bodies of muds (mainly silts), up to 0.2 m thick, are interbedded within facies Gm and Gh.

Unit 2 is approximately 22 m thick in both sections. This is an heterolithic interval with a clear predominance of sandy facies. Gravels are minor in LB2, while silts and clays become more abundant than in LB1. Sands form tabular strata, cm to dm thick, and display a wide array of facies (Sm, Sr1, Sr2, Sh, St and Ss); in-phase and in-drift climbing ripple lamination (type C of Jopling and Walker, 1968; or type 1 of Reineck and Singh, 1980; or type B of Ashley, 2002) is a noticeable feature. Gravels, with clasts up to 10 cm long, constitute wedge-shaped bodies up to 0.5 m thick in section LB1 that become thinner or pass laterally into finer facies in section LB2; most common facies are Gm, Gh, Gt and Gf. In all cases, sand- and gravel-size deposits wedge out southeastward (from LB1 to LB2), as the thickness of finer-size deposits increases, which indicates the transport direction of sediment. Well-sorted sands from three levels in Unit 2 were samples for OSL dating. Silts and clays form tabular or wedge-shaped intervals up to 3 m thick and show a great variety of facies, both structureless and with ripple and horizontal lamination. Fine, rhythmic lamination (Clh) is more noticeable towards the upper part of this unit, in particular in section LB2, where laminated intervals can be up to 5 m thick. In many cases, deformation structures (e.g., flames, contorted laminae

242 and micro-grabens) are present. Dropstones, mm to cm long, are common within silt
243 and clay facies (Fig. 7B, F).

244 Unit 3 consists of a slightly wedged, massive body, up to 6.5 m thick in section LB1,
245 mostly formed of structureless gravels (facies Gm, and minor Gh) with occasional, 0.3
246 m thick, lenticular bodies of sands (St, Sh). Clasts are up to 25-28 cm long in LB1 and
247 decrease to 20-23 cm in LB2.

248 Unit 4 is about 5 m thick in LB1 and 10.5 m thick in LB2. In LB1, it is formed of tabular
249 gravel bodies (facies Gm and Gh, with clasts up to 20 cm long) that alternate with
250 laminated clay intervals (Clh, up to 1.1 m thick) that contain dropstones up to 43 cm
251 long. In LB2, thin gravel (dm thick; clast size < 10 cm) and minor sand beds are
252 interbedded within thicker (up to 4 m minimum, at the base of Unit 4) clay intervals,
253 making a coarsening upward sequence.

254 Unit 5 is about 10 m thick in LB1 and 5 m thick in LB2. It is mostly made of massive
255 gravels (facies Gm and minor Gh), with clasts up to 20-25 cm in LB1 and 40 cm in LB2,
256 and occasional, decimetre-thick, lenticular sand beds (facies Sm and Sh) at the base.

257 4.2 Facies associations

258 Lateral and vertical relationships between the sedimentary facies can be expressed by
259 up to twelve facies associations (FA), i.e., simple vertical sequences (Fig. 10), that
260 correspond to three main depositional environments/settings: i) fluvial (braided river),
261 ii) lake margin (deltaic foresets and prodelta and subaqueous mass flows), and iii)
262 distal lake area or lake bottom plain (offshore areas). The main facies and facies
263 associations along the stratigraphic sections are indicated in Figure 3.

4.2.1 Fluvial facies associations (FA 1A and 1B, Fig. 10).

a) FA 1A [Gm -> (Gp—Sp), (Gt—St) -> Gh <-> (Sm, Sh) -> Fm]. This fining-upward FA represents deposits of a braided streams with longitudinal and transverse bars (Gh, Gp and Sp), shallow channels that can be filled with sinuous-crested dunes (Gt and St; Miall, 1977; Allen, 1982a, b), and sand sheet deposits (Sm and Sh). Massive fines (Fm) are very rare and form very thin deposits, representing waning of currents. Their scarcity probably was due to the small size of the floodplain and/or common erosional processes over this narrow valley area (cf., Arenas et al., 1989). These features along with the textural attributes (e.g., poor sorting and low roundness) suggest that the sequence represents sedimentation in a high energy braided fluvial system close to the sediment source area (i.e., equivalent to proximal to middle “outwash plain”). Unit 1 in the two sections LB1 and LB2 is formed of several fining-upward sequences that correspond to either the complete or incomplete FA 1A (Fig. 5A, B).

b) FA 1B [Gh, Sh -> (St), (Sm) -> Gm]. This coarsening-upward FA represents progradation of the fluvial system, with gravel beds (Gm, from flash floods) over small sand or gravel bedforms (Sh, Sm or Gh, from longitudinal and crescent bars), mostly developed under subaerial conditions. FA 1B is recognized in Units 3 and 5.

4.2.2 Lake margin associations: coarsening upward (deltaic and subaqueous mass flows) and fining upward (turbidite-like deposits) facies associations.

a) *Coarsening upward associations* (FA 2A, 2B and 3A, Fig. 10).

FA 2A [(Fh, Sh) -> Sr1, Sr2, (Sm) -> Gf—Sf] consists of gravel and sand foreset stratification overlying rippled and laminated sands and silts. It represents deposition

of small gravel and coarse sand bars that prograded on the lake margin, forming foresets (Gf and Sf) that suggest that sediments delivered to the delta avalanched and rolled down the delta front (Johnsen and Brennand, 2006; Winsemann et al., 2007). This FA is well developed at the base of the studied succession (between sections LB1 and LB2; Figs. 3, 4B, 5F to 5H) and in Unit 2 (Fig. 6F).

FA 2B [Clm <-> Fh, Clh <-> Sr1, Sr2, Fm] corresponds to prodelta deposition, relating to fine sandy and silty sediment that flowed down the delta front as hyperpycnal flow (e.g., Kostic et al., 2005; Johnsen and Brennand, 2006). Climbing ripples in FA 2 (Fig. 6B) provide evidence of rapid deposition from sediment-laden unidirectional flows in a standing body of water (Jopling and Walker, 1968; Allen, 1970, 1971; Stanley, 1974; Pietras and Carrol, 2006). The general coarsening upward evolution is due to delta progradation during increased sediment inputs. This FA is present in Unit 2 at section LB1.

FA 3A [Fm, Fh, Fr -> Gh, Sh -> Gm] was formed by suspension setting and low energy traction currents (Fm, Fh, Fr), followed by rapid deposition from high-velocity expanding jets that carried medium to coarse sediment (Gm, Gh, St, Sh, Sm) onto the lake margin. The coarser deposits (Gm) may correspond to debris-flow deposits (e.g., Winsemann et al., 2007; Evans et al., 2013) and other unconfined gravity flows (e.g., as described by Ashley, 2002). This FA is present in Unit 2 in section LB1 (Figs. 3, 7A).

b) *Fining-upward associations* (FA 4A, Fig. 10).

FA 4A [Gm, (Gh) <-> Clm -> Clh] resulted from deposition of sediment from meltwater streams that entered the lake as density currents forming coarse sediment drapes or

lobes (Gm and Gh), and fine sediment deposits from suspension settling (Clm and Clh) in a relatively deep water body, as evidenced by dropstones in the clay facies. This FA represents deposition from dense turbidity currents (Gruszka, 2007; Eyles and Eyles, 2010) in middle to distal lake areas. This FA is recognized in Unit 4 (LB1 and LB2) (Figs. 3, 7B).

4.2.3 Distal lake associations.

a) *Coarsening-upward associations* (FA 2C, 3B and 5, Fig. 10).

FA 2C [Fr, Sh -> Ss -> Sr2, St—(Gt)] (Fig. 6E) and 3B [Fh <-> Clh -> Sm, Sh <-> Gm] represent lacustrine deposition from highly energetic flows that reached distal deltaic areas that had previously been sites for fine deposition (facies Fr, Fh, Clh). These underflows gave rise to silty and sandy bedforms (Sr2 and St), including scour and fill structures (i.e., Ss in sequence 2C). In addition, sheet-like density flows that carried sand and fine gravel formed tabular beds (Sm, Sh and Gm) located at the top of sequence 3B.

FA 5 [Clm -> (Clh) -> Fm -> Sm] represents deposition in a more distal area and/or corresponds to lower-competence flows, compared to FA 2C and 3B. Facies Clm, Fh and Clh at the base of the three FA indicate fine sediment deposition from suspension by settling. Thick and extensive fine deposits formed during periods of high water level in the lake, when the lake was larger.

b) *Fining-upward and rhythmic associations* (FA 4B, 6A and 6B, Fig. 10).

These FA are characterized by having dominant fine sediments that show thin lamination or are structureless (Fig. 7C-F). These fine sediments (facies Fm, Clm and Clh) formed mainly by settling from suspension in offshore areas. Lamination in these fine grained deposits is formed of rhythmites (Fig. 8A, B), which consist of alternating thin silt laminae (submillimetre-thick) and thicker clay laminae (submillimetre- to millimetre-thick), or solely clay laminae of different colours. Some laminae show gradual fining-upward evolution from silt to clay, but commonly the two grain-size intervals are clearly separated (Fig. 8C). Sand-size grains in facies Clh correspond to angular dropstones (Fig. 8D). These rhythmites suggest the absence of significant coarse or middle-size sediment input that reached the lake centre, thus with coarse sedimentation likely limited to the lake margins. Probably, each rhythmite pair corresponds to a pulse of meltwater input, as proposed for some lake deposits (Desloges, 1994), but it can also result from deposition by distal turbidity currents without seasonal control (Ashley, 2002). In turn, the deposits of facies Sm, Sh, Sr and Fr in FA 4B and 6A indicate that current dynamics reached the distal lake areas, likely as density currents (e.g., as reported by Krzyszkowski, 1994; Gruszka, 2007). Thus, these sequences would reflect the succession or alternation of hyperpycnal flow turbidites (producing sandy deposits) and the tail of turbidity currents or quiet-water deposition from suspension (producing laminated silts and clays), as reported by Johnsen and Brennand (2006). In addition, ice-rafted dropstones, submillimetre to rare centimetre long, though not abundant, caused soft deformation of the laminae (Fig. 8D; e.g., as described by García et al., 2015). Rhythmic laminated silts and clays are common in many Pleistocene glacial lakes (e.g., Gruszka, 2007; Evans et al., 2013; Smith, 2017).

Deformation structures are present in almost all facies types. These structures include intraformational folds (cm to m high) in gravel and sand deposits (Fig. 9A, B), convoluted lamination/bedding in sandy to muddy deposits and sand and silt flames (Fig. 9D-F), and rare micro-faulting in sandy and muddy deposits (Fig. 9C), which together denote deformation driven by depositional, climate (controlled by melting-freezing processes of porewater) and/or tectonic (seismic) factors (Gruszka, 2001; Smith, 2017). Evidence for seismic origin is not always clear and many deformation structures might have been related to climatic and depositional processes. Soft sediment deformation structures in silt-rich sediment can be caused by overpressuring of porewater during freezing (Eyles and Eyles, 2010; Smith, 2017), and also can form during fluid escaping from sediments that have been deposited rapidly (Cheel and Rust, 1986; Prior and Bornhold, 1988; Johnsen and Brennand, 2006; Evans et al., 2013). The asymmetric deformation shapes of ripples, ripple lamination and sand and silt convolution in the study area suggests a flow component that is parallel to sediment transport direction, and thus indicates the effects of traction currents over soft sediment deposited at high rates (Fig. 9D).

4.3 Depositional environment evolution

Geomorphologic, stratigraphic and sedimentologic information allows us to reconstruct depositional evolution of the glaciofluvial and glaciolacustrine systems of Linás de Broto through time (Fig. 11). The ice tongue of the Ara trunk glacier dammed a braided gravelly fluvial system that was fed by meltwater from a small glacier that was present in the headwater of the River Sorrosal tributary valley. As a result, an extensive proglacial fluvial and lacustrine depositional system was developed near

374 Linás de Broto (Figs. 2A, 11, 12). The system was also fed by slope runoff and sediment
375 derived from the whole watershed. Only minor inputs from the Ara glacier (through
376 icebergs and meltwater transporting particles from the Viu moraine) are inferred from
377 the lithological nature (granite) of some clasts in gravels. The lake was approximately
378 0.5 km wide and 1.5 km long (minimum dimensions, based on extent of present
379 outcrops).

380 Unit 1 is referred to as FA 1A (Fig. 10) and represents deposition in shallow bars and
381 channels of a braided fluvial system (outwash train) with dominant subaqueous
382 traction of high competence and capacity. Similar deposits have been reported from
383 proximal and proximal-middle sectors of glaciofluvial systems (Evans et al., 2013;
384 García et al., 2015). The presence of vertical clasts indicates dispersive pressure after
385 deposition in high energy conditions (Allen, 1981). Erratics (single clast up to 1.2 m
386 long, Fig. 5E) support the association of these deposits within a glacial setting, as these
387 clasts only could be transported as sediment within floating- or rafting-ice masses
388 carried by the fluvial currents. The fluvial system also formed small coarse gravel
389 deltaic lobes (FA 2A, Fig. 10) that extended eastward and southeastward into the lake
390 (i.e., deposits that crop out below Unit 1, between sections LB1 and LB2; Figs. 3, 4B,
391 5F), as indicated by facies distribution through space and bedform palaeocurrents.

392 The general vertical sedimentary evolution of Unit 1 is fining upward. The clast size
393 decreases and the amount of sand-size facies increases from LB1 to LB2. Together, the
394 vertical and lateral evolution can be interpreted as a retrogradation stage of the fluvial
395 system following peak deposition that occurred in high energy conditions.

In Unit 2, FA are varied and correspond to both marginal (FA 2A, 2B, 3A and 3B) and distal lake deposits (FA 2C, 4B, 5, 6A and 6B) (Fig. 10). As a whole, the deposition of Unit 2 is mostly related to coarse sedimentation on the lacustrine margin (i.e., as small deltaic lobes, FA 2A, and gravity deposits from unconfined flows, FA 3A and 3B) and finer sedimentation towards more internal lacustrine zones (i.e., to more dilute bottom flows and settling out). Fine sand and silt facies intercalated within laminated clay sediments formed by settling out in offshore lacustrine zones (Fig. 11A, stage 2). These facies and the associated processes have been recognised in some ice-contact lakes (Ashley, 2002) that receive coarse detrital inputs.

The sharp contact between Units 1 and 2 (with respect to lithology, with Unit 2 beginning with fines over gravels of Unit 1) represents rapid lake expansion. The general vertical sedimentary evolution of Unit 2 is first coarsening-upward, then fining-upward. In the lower half, coarsening-upward sequences are dominant; the rest is composed of both fining- and coarsening-upward sequences, although coarsening-upward sequences dominate in LB1. As a whole, these features suggest progradation followed by retrogradation of the fluvio-deltaic system in the context of a general expansion of the lake, which is consistent with the increased thickness and abundance of fine sediment deposits (i.e., facies Clm, Clh and Fm) and decreased thickness and abundance of coarse facies toward the upper half of this unit.

Unit 3, mostly formed of massive gravels with occasional sands, is characterized by FA 1B. Deposition of this unit is related to a period of high discharge of the fluvial system. The vertically orientated clasts confirm dispersive processes and rapid deposition in high energy conditions (Allen, 1981), i.e., upward orientation of the clasts under the

influence of high pressure through fluidized sediment. Together, deposition of Unit 3 represents the invasion of a large extent of the lake area with alluvial deposits. This drastic lake-area reduction or even disappearance could be concurrent with a lowering of the lake level (Fig. 11B, stage 3).

Unit 4 deposits, represented by FA 6B, 6A and 4A (Fig. 7B, D-F), formed following a very rapid lake expansion; on the lake margins, coarse sediments deposited from unconfined bottom flows could reach more internal zones. In these inner lacustrine zones, settling from suspension was the dominant process (e.g., as represented by stage 2 in Fig. 11A). Unit 4 shows a sharp basal contact with the underlying gravels.

Unit 5, formed of massive gravels (FA 1B), together with Unit 4, constitute a coarsening upward macrosequence resulting from progradation of the fluvial system that entered the lake. The massive character of this unit reflects dominant flash flood processes associated with intense meltwater currents that extended southeastward, and coincided with the final fill of the lake. Stage 3 in figure 11B would represent the beginning of such scenario.

In summary, the general evolution of the two sections reflects a complex expansion-retraction process of the lake that occurred in parallel with a complex retrogradation-progradation process of the high-energy braided fluvial system that entered the lake (Fig. 11). Section LB1 records deposition in more proximal zones, both in fluvial and marginal lacustrine settings, while section LB2 reflects more distal sedimentation of the fluvial system (e.g., as dense bottom flows) and primarily offshore lacustrine, in many cases rhythmic, sedimentation by settling during lake expansion stages.

441 Final fill of the depositional area coincided with progradation of the fluvial system and
442 lake opening by failure of the Ara glacier ice and moraine dam; subsequently, fluvial
443 incision of the Viu moraine and of the Q1 deposits started.

444 ***5. OSL chronological data***

445 Results from optically stimulated luminescence (OSL) dating of three samples from
446 section LB1 (Fig. 3) and one sample from the terrace kame deposits that laterally
447 overlie the Viu moraine (A1.c in Fig. 2B) are discussed here (Table 2). Samples X1600
448 (metre 21 of Unit 2) and X1598 (metre 33-34 of Unit 2) provided age estimates in the
449 correct stratigraphic order: 55±9 ka, and 49±11 ka, for the middle and upper parts,
450 respectively, of Unit 2 in section LB1 (Fig. 3). Sample X1599, between these two,
451 provided an apparent age of 82±6 ka. Probably the age provided by sample X1599 is
452 overestimated, given its stratigraphic position relative to the other dated samples,
453 which provided age estimates consistent with each other. Sample X1601, from the
454 terrace kame deposits, gave an age estimate of 49±8 ka, which is consistent with the
455 top of Unit 2 in the Linás de Broto sequence (Table 2). Therefore, the Viu moraine
456 started to form slightly before that age. These ages are older than the age obtained by
457 Martí-Bono et al. (2002) (30.4±0.4 ka BP) for this lacustrine record using AMS
458 radiocarbon dating on concentrated pollen samples in a position equivalent to Unit 2.
459 However, the age obtained by Martí-Bono et al. (2002) should be taken with caution
460 because of 1) the difficulty to use concentrated pollen for AMS radiocarbon dating,
461 and 2) the age of the samples is close to the limit of application of this technique.

462 The analysed samples provided low yields of quartz grains, and also display relatively
463 low signal sensitivity, variable and occasionally high levels of Infra-Red Stimulated
464 Luminescence (IRSL, associated with feldspar grains or micro-inclusions), with poor
465 recycling and/or high levels of thermal transfer for several aliquots. These
466 characteristics are not ideal for OSL dating, leading to some caution in the
467 interpretation of the results. However, the apparent agreement between three of the
468 four samples dated suggests that the quartz grains in this area can provide age
469 estimates that in general are internally consistent and are considered broadly reliable.
470 Low sensitivities of these glaciogenic samples are likely related to relatively brief
471 transport of the constituent grains since excavation from bedrock. For some samples, a
472 small number of aliquots showed significantly higher D_e values than others. These are
473 interpreted as representing occasional grains which had been insufficiently zeroed
474 during sedimentation (short transport in high-turbidity flow conditions and sometimes
475 beneath ice-cover) and they have been omitted for age calculations. Similar findings
476 are also observed in other glaciated regions, including the Himalayas (Rhodes and
477 Pownall, 1994) and Greenland (Rhodes, 2000).

478 **6. Discussion**

479 Geomorphologic evidence supports the hypothesis that the lateral moraine preserved
480 close to the Viu village (Fig. 2A) corresponds to the maximum extent of the Ara glacier
481 during the LGC (García-Ruiz and Martí-Bono, 1994). At this point the ice tongue coming
482 from the Vignemale massif terminated around the Asín de Broto village (Serrano and
483 Martínez de Pisón, 1994) (Fig. 2C). These authors proposed, based on morphological
484 features and regional studies, that this ice advance was prior to LGM (point 3 in Fig.

485 1B). Other more internal lateral moraines (e.g., the Fragen moraine, Fig. 2A) in this
486 sector of the River Ara valley represent a subsequent retreat stage of the glacier
487 (García-Ruiz and Martí-Bono, 1994). The Ara trunk glacier dammed a glaciolacustrine
488 depositional system related to the maximum ice extent during the Last Glacial Cycle.
489 Despite uncertainty of the obtained datings, it can be proposed tentatively that the
490 studied sedimentary sequence lasted from Marine Isotope Stage 4 (MIS4, prior to 55±9
491 ka BP) to the middle MIS3 (approximately 49±11 ka BP). Together, these results allow
492 two main points to be discussed below: 1) The climatic and hydro-climatic conditions
493 during this period inferred from the evolution of the depositional sedimentary system,
494 and 2) The significance of the maximum ice surface extent of the Ara glacier during the
495 LGC at a regional scale.

496 ***6.1. Evolution of the glacio-fluvio-lacustrine depositional system of Linás de Broto***

497 The stratigraphic and sedimentologic characteristics of the fluvial and lacustrine record
498 at Linás de Broto suggest a complex sedimentary evolution resulting from an
499 expansion-retraction cycle of the lake, parallel to a retrogradation-progradation cycle
500 of the high-energy braided fluvial system entering the lake (Fig. 11). This evolution
501 implies changes in watershed hydrology, lake hydrology and sediment supply that
502 were triggered by climate conditions in the context of the maximum glacier advance
503 during the LGC in the south-central Pyrenees.

504 Deposition of Unit 1 was produced in shallow bars and channels in a high energy
505 braided fluvial environment. This environment developed as a narrow outwash train in
506 front of the Sorrosal glacier. Small gravelly and sandy deltaic lobes formed on the

507 northern lakeshore areas (e.g., FA 2A). Most of this coarse sediment originated from
508 melting of ice masses that dragged and transported till deposits of the Sorrosal glacier
509 (Figs. 11, 12). Sediments were also derived from the hilly slopes throughout the valley.
510 From clast composition (with very rare granite clasts carried by the Ara glacier from
511 the Pyrenean Axial Zone), it can be deduced that only a very small proportion of
512 sediments into the depositional system derived from the trunk Ara glacier via its lateral
513 moraine (e.g., via ice sliding that would form icebergs in the lake). These processes
514 imply a low water lake level (Fig. 12A), i.e., a lowering with respect to levels during
515 deposition of Units 2 and 4 (Fig. 12B). The Viu moraine (A1 in Fig. 2B) was built, at least
516 partially during Unit 1 deposition.

517 According to the age estimates obtained, the fluvial depositional phase of Unit 1
518 occurred before 55±9 ka BP, at the end of the MIS4 or very close to the MIS4-MIS3
519 transition (approximately at 59 ka after Martinson et al., 1987), considering the global
520 boundaries between events provided by Lisiecki and Raymo (2005). In the valleys of
521 the Cinca and Gállego rivers (Fig. 1), Lewis et al. (2009) linked fluvial aggradation
522 phases during the mid-late Pleistocene to enhanced periods of glacier melting that
523 produced massive discharges of water and sediment downstream along the valleys.
524 These meltwater discharge processes were related to periods of maximum summer
525 insolation during cold and transitions from cold to deglaciation phases (Lewis et al.,
526 2009). High geomorphic significance can be attributed to the glacial stage at 64±11 ka,
527 recorded in the terminal moraine of Salinas de Sin, in the Cinca/Cinqueta valley (MIS4;
528 4a in Fig. 1B), and the correlated Qt7 terrace in the River Cinca valley (4b in Fig. 1B) at
529 61±4 ka (Lewis et al., 2009). The relationship between increased fluvial aggradation

530 and high summer insolation periods is also shown by Benito et al. (2010) in the River
531 Gállego valley.

532 Thus, the deposition of Unit 1 in Linás de Broto could be related to this regional fluvial
533 aggradational period. In this context, the deposits at Linás de Broto preserve a record
534 of higher frequency changes: periods with high summer insolation (i.e., associated with
535 an increase of alluvial sediment supply) and periods with reduced summer insolation
536 (i.e., associated with a decrease of melting water). In this way, Units 3 and 5 of
537 sections LB1 and LB2 (Fig. 3) represent short fluvial progradation phases (e.g., stage 3
538 in Fig. 11B) that may be related to periods of maximum summer insolation that
539 provided low ratios of water discharge vs. sediment flux.

540 The deposits of Units 3 and 5 clearly indicate a southeastward progradation of the
541 fluvial system that ended up with size reduction of the lake surface and maybe the
542 final lake filling episode (Fig. 12A). Considering the age of Unit 2 (from 55±9 to 49±11
543 ka BP), the deposits of Units 3 to 5 were likely deposited during MIS3 (this stage lasted
544 approximately from 59 to 24 ka, after Martinson et al., 1987). This MIS encompasses
545 several global stadial phases (Rasmussen et al., 2014), as well as a general maximum
546 summer insolation in the northern hemisphere (Berger and Loutre, 1991).

547 In contrast, deposits of Units 2 (55±9 to 49±11 ka BP) and 4 (Fig. 3) represent rapid
548 expansion stages of the lake (e.g., as evidenced through sharp contact between
549 underlying coarse deposits and fine sediments containing dropstones) and coincide
550 with the retrogradation of the fluvial system (Figs. 11A, 12B). Structureless clays may
551 record long periods without, or with only minor, coarse sediment supply to the

552 expanded lake. These observations could be interpreted as a high ratio of water
553 discharge vs. sediment flux. However, lake expansion was primarily caused by rapid
554 and prolonged closure of the lake by the lateral moraine and ice growth of the Ara
555 glacier, likely during relatively colder conditions, and probably coinciding with low-
556 insolation summer periods. In this context, very fine, mostly rhythmic lamination and
557 dropstones would form during relatively short (i.e., seasonal) climate fluctuations.
558 However, the possibility that these laminites represent varves is ruled out because ice-
559 contact lakes are not fully sensitive to seasonal changes in temperature (cf., Ashley,
560 2002). Moreover, the irregular variations of lamina thickness through time and
561 abundance of turbidite-like deposits within the Linás de Broto offshore sequence
562 support non-seasonal/non-periodic sediment inputs to the lake.

563 Given the different deposition rates inferred from the sedimentary attributes (e.g.,
564 fluvial and deltaic deposits versus laminites) of Units 1, 3 and 5 compared to Units 2
565 and 4, it can be suggested that the deposition of gravelly sediments or fluvial
566 progradation occurred during short periods characterized by dominant high summer
567 insolation, which favored ablation and sediment production. In contrast, lake
568 expansion occurred during longer periods with dominant low summer insolation,
569 which decreased ablation and sediment production. This sedimentary scenario was
570 made possible as a consequence of lake closure by the Ara trunk glacier.

571 ***6.2. Palaeoclimatic implications: the maximum ice extent during the Last Glacial***
572 ***Cycle in the Pyrenees***

573 The timing of the maximum ice extent through the LGC (130-14 ka, according Gibbard
574 and Cohen, 2008) and the occurrence of the LGM (≈ 23-19 ka, according Hughes et al.,
575 2013) in the south Pyrenees have been persistent matters of debate. Indirect dates
576 from lacustrine records (Montserrat-Martí, 1992; García-Ruiz et al., 2003; González-
577 Sampériz et al., 2006), and optically stimulated luminescence (Sancho et al., 2003;
578 Lewis et al., 2009; García-Ruiz et al., 2013) and terrestrial cosmogenic nuclides (TCN)
579 dates (Delmas et al., 2008; Pallás et al., 2010; Calvet et al., 2011) confirmed the
580 asynchronous nature of the regional maximum glacier advances in respect to global
581 glaciations.

582 In this work, the occurrence of a maximum ice extent of the Ara glacier prior to 51±9
583 ka (age from the three reliable OSL dates; Table 2) during the LGC has been reported. It
584 has a regional expression that is documented in the different south-central Pyrenean
585 glaciated valleys (e.g., points with datings in Fig. 1B, Table 3). Of these, the terminal till
586 of Salinas de Sin (point 4a in Fig. 1B), gave an OSL age of 64±11 ka (Sancho et al., 2003,
587 2004; Lewis et al., 2009). In the Sabiñánigo sector of the River Gállego valley, extensive
588 fluvio-glacial terraces (point 2b in Fig. 1B) yielded OSL ages ranging between 62.7±3.9
589 and 69±8 ka (the preferred combined age is 68±7 ka; Peña et al., 2004; Lewis et al.,
590 2009). A terminal moraine at Castiello de Jaca (River Aragón valley, also to the west of
591 the River Ara valley; point 1b in Fig. 1B) showed an OSL age of 68±7 ka (García Ruiz et
592 al., 2013).

593 Farther east, using ^{10}Be exposure ages, Pallàs et al. (2010) found that the maximum
594 glacial extent in some eastern Pyrenean valleys (e.g. Carol and Malnuy valleys) may
595 have occurred during MIS4 (approximately 74-59 ka, after Martinson et al., 1987).

596 Similarly, in the River Valira valley, Andorra (point 5 in Fig. 1B), Turu et al. (2017)
597 placed the Würmian maximum ice extent at 59±1.18 ka, an age obtained from
598 cosmogenic isotope analyses applied to a glacially-polished rock surface. Nevertheless,
599 Pallás et al. (2006), using also exposure ages on boulders and glacial erosion landforms,
600 indicated that pleniglacial conditions in the eastern Pyrenees could have occurred over
601 a long period (from 30 to 20 ka), including several glacier advances and retreats, with a
602 last maximum glacier advance during the LGM (≈ 18 ka ago). Delmas et al. (2008), by
603 using cosmogenic dates, also reported the maximum ice advance to have occurred
604 during the LGM in the eastern Pyrenees. Calvet et al. (2011) and Delmas et al. (2011)
605 also confirmed the asynchroneity of the maximum ice extent during the LGC in the
606 Pyrenees.

607 Thus, the maximum ice extent during the LGC in the central Pyrenees is older than
608 LGM, whereas in the eastern Pyrenees it occurred later, coinciding with the LGM.
609 Consequently, a non-uniform behaviour represented by the extent of glaciers, both
610 from Northern Europe to Iberian Peninsula (latitudinal/global scale) and from west to
611 east along the Pyrenees (longitudinal/regional scale) could be stated.

612 It is not easy to explain this asynchronous global and regional nature of the maximum
613 glacier advances during the LGM at the Pyrenees. The different latitudinal response of
614 the Pyrenean glacial systems respect to the northernmost continental ice-sheets (e.g.,
615 Ehlers and Gibbard, 2004) may be explained by the southern latitude of the Pyrenees
616 (Florineth and Schlüchter, 2000; García-Ruiz et al, 2003). Low-latitude climate in the
617 southern North-Atlantic appears to be very sensitive to the latitudinal shifts of the
618 Polar Front controlling the westerlies regime in the North Atlantic (Calvo et al., 2001;

Eynaud et al., 2009; Domínguez-Villar et al., 2013). A southernmost position of the Polar Front during the LGM (MIS2), located between 37°N and 43°N (Calvo et al., 2001), would restrict the advance of the south-central Pyrenean glaciers due to the decreased precipitation (Florineth and Schlüchter, 2000; Sanchez-Goñi et al., 2008), probably associated with the low sea-surface temperature in comparison with other periods (Domínguez-Villar et al., 2013). Consequently, cold and arid conditions prevailed during the LGM in the Pyrenees, as deduced from palynological records (Jalut et al., 1992). However, discrepancies about the position of the Polar Front and the derived sea-surface temperature have been observed. For example, Eynaud et al. (2009) indicate that the Polar Front did not reach the Iberian Peninsula during the LGM and a northward advance of warm waters is proposed.

Latitudinal migrations of the Polar Front during LGM affecting the western Iberian margin imply changes in the sea surface temperature (SST). But, controversy also appears when SSTs are estimated. Calvo et al. (2001) indicate SSTs of 8-10°C at 43°N during the LGM. SSTs of 2 to 4°C lower than at present have been reconstructed by Waelbroeck et al. (2014). However, this difference is lower (≈ 1 to 2°C) according to Eynaud et al. (2009). Regardless, this difference is minimal for mean estimated summer SST at 43°N in the western Iberian margin (present is 17.8°C, and LGM estimate is 17.4°C) (Salgueiro et al., 2010).

The asynchronous regional extent of glaciers from central to eastern Pyrenees could be related to the increase of snow precipitations in the eastern Pyrenean sector, compatible with a more southerly position of the Polar Front, but also consistent with a strengthening of the low pressure systems in a warmer western Mediterranean sea

642 compared to a cooler southern North-Atlantic ocean during the LGM (Delmas et al.,
643 2011). Delmas et al. (2011), based on temperature reconstructions from diverse
644 proxies by Hayes et al. (2005) and de Vernal et al. (2005), suggest mean annual SSTs of
645 13-14.5°C in the Balearic area, and of 6.3-7.6°C in the Bay of Biscay. Other
646 reconstructions of SSTs during the LGM in the western Iberian margin and the western
647 Mediterranean show an attenuation of the temperature gradient between these areas
648 due to a reorganization of surface water circulation in the western Mediterranean and
649 a reduction in the inflow of Atlantic water (Waelbroeck et al., 2014).

650 **7. Conclusions**

651 The geomorphology, stratigraphy and sedimentology, along with chronology of the
652 glacio-fluvio-lacustrine sequence at Linás de Broto (south-central Pyrenees,
653 Northeastern Iberian Peninsula) allow us to characterize the evolution of the
654 depositional system as well as to derive regional climate implications for late
655 Pleistocene.

656 1) The sequence, ≈ 55 m thick, is divided into five lithological units that formed in three
657 main environments: gravel braided system (outwash train), lake margin (gravel and
658 sand deltas and fans) and distal lake or lake bottom plain (e.g., rhythmites, from distal
659 hyperpycnal flows and dominant settling from suspension). Twelve facies associations
660 represent the sedimentation variations through time in these settings.

661 2) The age estimates obtained within the middle portion of the sequence (Unit 2)
662 range from 55±9 ka to 49±11 ka. Thus, the sequence developed during MIS4 and,
663 partially, MIS3. The occurrence of this depositional system is related to the maximum

ice extent of the Ara trunk glacier during the Last Glacial Cycle. These dates confirm the early age (during MIS4) of the maximum ice extent of the south-central Pyrenean glaciers. The asynchronous response of the Pyrenean glacial systems respect to Northern Europe glaciers seems related to the position of the Polar Front in the western Iberian margin through its influence on precipitation during the LGM.

3) The evolution of the studied environments over the period of maximum ice extent in the south-central Pyrenees is consistent with a complex expansion-retraction lacustrine stage that paralleled a complex retrogradation-progradation stage of the fluvial system. Fluvial progradation may be related to short periods of ice melting, while lake expansion concurred with ice-dam growth in the trunk glacier during longer periods. Thus, the development of proglacial, glaciolacustrine environments can be sensitive to variations in summer insolation regulated by orbital forcing.

Acknowledgments

This study is a contribution of the research groups *Paleoambientes del Cuaternario*, *Análisis de Cuencas Sedimentarias Continentales* and *Geomorfología y Cambio Global* (Aragon Government and European Social Fund) and of the Environmental Sciences Institute of the University of Zaragoza (IUCA). The authors would like to thank he *Servicios de Apoyo a la Investigación* (SAI) of the University of Zaragoza (Spain). An anonymous reviewer and editor Dr. Knight helped improve the manuscript.

References

Allen, J.R.L., 1970. A quantitative model of climbing ripples and their cross-laminated deposits. Sedimentology 14, 5-26.

686 Allen, J.R.L., 1971. Instantaneous sediment deposition rates deduced from climbing
687 ripple cross-lamination. Journal of the Geological Society of London 127, 553-561.

688 Allen, J.R. 1982a. Sedimentary structures: their character and physical basis, volume I.
689 Developments in Sedimentology 30A, Elsevier, Amsterdam, 593 pp.

690 Allen, J.R. 1982b. Sedimentary structures: their character and physical basis, volume II.
691 Developments in Sedimentology 30B, Elsevier, Amsterdam, 663 pp.

692 Allen, P.A., 1981. Sediments and processes on a small stream-flow dominated,
693 Devonian alluvial fan, Shetland Islands. Sedimentary Geology 29, 31-66.

694 Arenas, C., Pardo, G., González, A., Villena, J., 1989. El sistema aluvial de Cobatillas
695 (Teruel): análisis de facies y evolución del estilo fluvial. Revista de la Sociedad
696 Geológica de España 2, 41-54.

697 Ashley, G.M., 2002. Glaciolacustrine environments. In: Menzies, J. (Ed.), Modern and
698 Past Glacial Environments. Butterworth-Heinemann, Oxford, pp. 335-359.

699 Barnolas, A., Pujalte, V., 2004. La Cordillera Pirenaica. In: Vera, J.A. (Ed.), Geología de
700 España. Sociedad Geológica de España-Instituto Geológico y Minero de España,
701 Madrid, pp. 233-241.

702 Barrere, P., 1963. La période glaciaire dans l'Ouest des Pyrénées centrales Franco-
703 espagnoles. Bulletin de la Société Géologique de France 7, 516-526.

704 Benito, G., Sancho, C., Peña, J.L., Machado, M.J., Rhodes, E.J., 2010. Large-scale karst
705 subsidence and accelerated fluvial aggradation during MIS6 in NE Spain: climatic and
706 paleohydrological implications. Quaternary Science Reviews 29, 2694-2704.

707 Berger, A., Loutre, M.F., 1991. Insolation values for the climate of the last 10 million
708 years. Quaternary Science Reviews 10, 297-317.

709 Blair, T.C., 1987. Sedimentary processes, vertical stratification sequences, and
710 geomorphology of the Roaring River alluvial fan, Rocky Mountain National Park,
711 Colorado. Journal of Sedimentary Petrology 57, 1-18.

712 Bordonau, J., 1992. Els complexos glàcio-lacustres relacionats amb el darrer cicle
713 glacial als Pirineus. Geoforma Ediciones, Logroño, 251 pp.

714 Bordonau, J., Vilaplana, J.M., Fontugne, M., 1993. The glaciolacustrine complex of
715 Llestui (Central Southern Pyrenees). A key locality for the chronology of the last glacial
716 cycle in the Pyrenees. Comptes rendus l'Académie des Sciences de Paris Série II, 316,
717 807-813.

718 Calvet, M., Delmas, M., Gunnell, Y., Braucher, R., Bourlès, D., 2011. Recent advances in
719 research on Quaternary glaciations in the Pyrenees. In: Ehlers, J., Gibbard, P.L.,
720 Hughes, P. (Eds), Quaternary Glaciations, Extent and Chronology, A Closer Look, Part
721 IV. Developments in Quaternary Science 15. Elsevier, Amsterdam, pp. 127-139.

722 Calvo, E., Villanueva, J, Grimalt, J.O., Boelaert, A., Labeyrie, L., 2001. New insights into
723 the glacial latitudinal temperature gradients in the North Atlantic. Results from $U^{K'}_{37}$

724 sea surface temperatures and terrigenous inputs. Earth and Planetary Science Letters
725 188, 509-519.

726 Carrasco, R.M., Pedraza, J., Domínguez-Villar, D., Villa, J., Willenbring, J.K., 2013. The
727 plateau glacier in the Sierra de Béjar (Iberian Central System) during its maximum
728 extent. Reconstruction and chronology. Geomorphology 196, 83-93.

729 Carrasco, R.M., Pedraza, J., Domínguez-Villar, D., Willenbring, J.K., Villa, J., 2015.
730 Sequence and chronology of the Cuerpo de Hombre paleoglacier (Iberian Central
731 System) during the last glacial cycle. Quaternary Science Reviews 129, 163-177.

732 Cheel, R.J., Rust, B.R., 1986. A sequence of soft sediment deformation (dewatering)
733 structures in late Quaternary subaqueous outwash near Ottawa, Canada. Sedimentary
734 Geology 47, 77-93.

735 Chueca, J., Peña, J.L., Lampre, F., García-Ruiz, J.M., Martí-Bono, C., 1998. Los glaciares
736 del Pirineo aragonés: estudio de su evolución y extensión actual. Departamento de
737 Geografía y Ordenación del Territorio. Universidad de Zaragoza, 104 pp.

738 De la Riva, J., 2000. Caracterización climática del alto valle de Tena. Boletín
739 Glaciológico Aragonés 1, 81-109.

740 de Vernal, A., Rossell-Melé, A., Kucera, M., Hillaire-Marcel, C., Eynaud, F., Weinelt, M.,
741 Dokken, T., Kageyama, M., 2005. Comparing proxies for the reconstruction of LGM sea-
742 surface conditions in the northern North Atlantic. Quaternary Science Reviews 25,
743 2820-2834.

744 Del Barrio, G., Creus, J., Puigdefábregas, J., 1990. Thermal seasonality of the high
745 mountain belts of the Pyrenees. Mountain Research and Development 10, 227-233.

746 Delmas, M., Calvet, M., Gunnell, M., Braucher, R., Bourlès, D., 2011. Palaeogeography
747 and ^{10}Be exposure-age chronology of Middle and Late Pleistocene glacier systems in
748 the northern Pyrenees: implications for reconstructing regional palaeoclimates.
749 Palaeogeography, Palaeoclimatology, Palaeoecology 305, 109-122.

750 Delmas, M., Gunnell, Y., Braucher, R., Calvet, M., Bourlès, D., 2008. Exposure age
751 chronology of the last glaciation in the eastern Pyrenees. Quaternary Research 69,
752 231-241.

753 Desloges, J.R., 1994. Varve Deposition and the Sediment Yield Record at Three Small
754 Lakes of the Southern Canadian Cordillera. Arctic and Alpine Research 26, 130-140.

755 Domínguez-Villar, D., Carrasco, R.M., Pedraza, J., Cheng, H., Edwards, R.L., Willenbring,
756 J.K., 2013. Early maximum extent of paleoglaciers from Mediterranean mountains
757 during the last glaciation. Scientific Reports 3, 2034, DOI: 10.1038/srep02034.

758 Ehlers, J., Gibbard, P.L. (Eds), 2004. Quaternary Glaciations. Extent and Chronology,
759 Part I: Europe. Developments in Quaternary Science 2, Elsevier, London, 488 pp.

760 Evans, D.J.A., Rother, H., Hyatt, O.M., Shulmeister, J., 2013. The glacial sedimentology
761 and geomorphological evolution of an outwash head/moraine-dammed lake, South
762 Island, New Zealand. Sedimentary Geology 284-285, 45-75.

763 Eyles, C.H., Eyles, N., 2010. Glacial Deposits. In: James, N.P., Dalrymple, R.W. (Eds.),
764 Facies models 4, Series GEOtext 6. Geological Association of Canada, Canada, pp. 73-
765 104.

766 Eynaud F., Abreu, L., Voelker, A., Schönfeld, J., Salgueiro, E., Turon, J.L., Penaud, A.,
767 Toucanne, S., Naughton, F., Sánchez-Goñi, M.F., Malaizé, B., Cacho, I., 2009. Position of
768 the Polar Front along the western Iberian margin during key cold episodes of the last
769 45 ka. Geochemistry, Geophysics, Geosystems 10, DOI: 10.1029/2009GC002398.

770 Florineth, D., Schlüchter, Ch., 2000. Alpine evidence for atmospheric circulation
771 patterns in Europe during the Last Glacial Maximum. Quaternary Research 54, 295-
772 308.

773 Fuller, I.C., Macklin, M.G., Lewin, J., Passmore, D.G., Wintle, A.G., 1998. River response
774 to high-frequency climate oscillations in southern Europe over the past 200 k.y.
775 Geology 26, 275-278.

776 García, J.L., Jorge A. Strelin, J.A., Vega, R.M., Hall, B.L., Stern, C.R., 2015. Deglacial ice-
777 marginal glaciolacustrine environments and structural moraine building in Torres del
778 Paine, Chilean southern Patagonia. Andean Geology 42, 190-212.

779 García-Ruiz, J.M., Martí-Bono, C., 1994. Rasgos fundamentales del glaciarismo
780 Cuaternario en el Pirineo aragonés. In: Martí-Bono, C., García-Ruiz, J.M. (Eds.), El
781 glaciarismo surpirenaico: nuevas aportaciones. Geoforma Ediciones, Logroño, pp. 17-
782 31.

783 García-Ruiz, J.M., Valero-Garcés, B.L., Martí-Bono, C., González-Sempériz, P., 2003.
784 Asynchroneity of maximum glacier advances in the central Spanish Pyrenees. Journal
785 of Quaternary Science 18, 61-72.

786 García-Ruiz, J.M., Martí-Bono, C., Peña-Monné, J.L., Sancho, C., Rhodes, E.J., Valero-
787 Garcés, B., González-Sampériz, P., Moreno, A., 2013. Glacial and fluvial deposits in the
788 Aragón Valley, central-western Pyrenees: chronology of the Pyrenean late Pleistocene
789 glaciers. Geografiska Annaler: Series A, Physical Geography 95, 15-32.

790 Gibbard, P., Cohen, K.M., 2008. Global chronostratigraphical correlation table for the
791 last 2.7 million years. Episodes 31, 243-247.

792 González-Sampériz, P., Valero-Garcés, B. L., Moreno, A., Jalut, G., García-Ruiz, J.M.,
793 Martí-Bono, C., 2006. Climate variability in the Spanish Pyrenees during the last 30,000
794 yr revealed by the El Portalet sequence. Quaternary Research 66, 38-52.

795 Gruszka, B., 2001. Climatic versus tectonic factors in the formation of the
796 glaciolacustrine succession (Bełchatów outcrop, central Poland). Global and Planetary
797 Change 28, 53-71.

798 Gruszka, B., 2007. The Pleistocene glaciolacustrine sediments in the Bełchatów mine
799 (central Poland): Endogenic and exogenic controls. Sedimentary Geology 193, 149-166.

800 Hayes, A., Kucera, M., Kallel, N., Sbaffi, L., Rohling, E.J. ,2005. Glacial Mediterranean
801 sea surface temperatures based on planktonic foraminiferal assemblages. Quaternary
802 Science Reviews 24, 999-1016.

803 Hughes, P.D., Woodward, J.C., 2008. Timing of glaciation in the Mediterranean
804 mountains during the last cold stage. Journal of Quaternary Science 23, 575-588.

805 Hughes, P.D., Gibbard, P.L., Ehlers, J., 2013. Timing of glaciation during the last glacial
806 cycle: evaluating the meaning and significance of the 'Last Glacial Maximum' (LGM).
807 Earth-Science Reviews 125, 171-198.

808 Hughes, P.D., Woodward, J.C., Gibbard, P.L., 2006a. Quaternary glacial history of the
809 Mediterranean mountains. Progress in Physical Geography 30, 334-364.

810 Hughes, P.D., Woodward, J.C., Gibbard, P.L., 2006b. Late Pleistocene glaciers and
811 climate in the Mediterranean. Global and Planetary Change 50, 83-98.

812 Jalut, G., Montserrat-Martí, J., Fontugne, M., Delibrias, G., Vilaplana, J.M., Julia, R.,
813 1992. Glacial to interglacial vegetation changes in the northern and southern Pyrenees:
814 Deglaciation, vegetation cover and chronology. Quaternary Science Reviews 11, 449-
815 480.

816 Jiménez-Sánchez, M., Rodríguez-Rodríguez, L., García-Ruiz, J.M., Domínguez-Cuesta,
817 M.J., Farias, P., Valero-Garcés, B., Moreno, A., Rico, M., Valcárcel, M., 2013. A review of
818 glacial geomorphology and chronology in northern Spain: Timing and regional
819 variability during the last glacial cycle. Geomorphology 196, 50-64

820 Johnsen, T.F., Brennand, T.A., 2006. The environment in and around ice-dammed lakes
821 in the moderately high relief setting of the southern Canadian Cordillera. Boreas 35,
822 106-125.

823 Jopling, A.V., Walker, R.G., 1968. Morphology and origin of ripple-drift cross
824 lamination, with examples from the Pleistocene of Massachusetts. Journal of
825 Sedimentary Petrology 38, 971-984.

826 Kostic, B., Becht, A., Aigner, T., 2005. 3-D sedimentary architecture of a Quaternary
827 gravel delta (SW-Germany): Implications for hydrostratigraphy. Sedimentary Geology
828 181, 143-171.

829 Krzyszkowski, D., 1994. Controls on sedimentation in the Elsterian proglacial lake,
830 Kleszczów Graben, central Poland. In: Warren, W.P., Croot, D.G. (Eds.), Formation and
831 Deformation of Glacial Deposits. Balkema, Rotterdam, pp. 53-68.

832 Lewis, C., McDonald, E., Sancho, C., Peña, J.L., Rhodes, E., 2009. Climatic implications of
833 correlated Upper Pleistocene glacial and fluvial deposits on the Cinca and Gállego
834 Rivers (NE Spain) based on OSL dating ans soil stratigraphy. Global and Planetary
835 Change 67, 141-152.

836 Lisiecki, L.E., Raymo, M.E., 2005. A Pliocene-Pleistocene stack of 57 globally distributed
837 benthic $\delta^{18}O$ records. Paleoceanography 20, PA1003, doi:10.1029/2004PA001071.

838 López, F., Cabrera, M., Cuadrat, J.M., 2007. Atlas Climático de Aragón. Departamento
839 de Medio Ambiente, Gobierno de Aragón, España, 213 pp.

840 Mallada, L., 1878. Descripción física y geológica de la provincia de Huesca. Memorias
841 de la Comisión del Mapa Geológico de España, Madrid, 432 pp., 1 mapa.

842 Martí-Bono, C., 1977. El valle de Hecho. Trabajos sobre Neógeno-Cuaternario 6, 349-
843 356.

844 Martí-Bono, C., 1996. El glaciarismo cuaternario en el Alto Aragón Occidental. PhD
845 Thesis, Universitat de Barcelona, 254 pp.

846 Martí-Bono, C., González-Sampériz, P., Valero-Garcés, B., García-Ruiz, J.M., 2002. El
847 depósito glaciolacustre de Linás de Broto (Pirineo aragonés) y su implicación
848 paleoambiental. In: Pérez-González, A., Vegas, J., Machado, M.J. (Eds.), Aportaciones a
849 la Geomorfología de España en el inicio del Tercer Milenio. Instituto Geológico y
850 Minero de España, pp. 77-83.

851 Martinson, D.G., Pisias, N.G, Hays, J.D., Imbrie, J., Moore, T.C., Shackleton, N.J., 1987.
852 Age dating and the orbital theory of the ice ages: Development of a high-resolution 0
853 to 300,000-year chronostratigraphy. Quaternary Research 27, 1-29.

854 Matthews, J.A., Dahl, S.O., Nesje, A., Berrisford, M.S., Andersson, C., 2000. Holocene
855 glacier variations in central Jotunheimen, southern Norway based on distal
856 glaciolacustrine sediment cores. Quaternary Science Reviews 19, 1625-1647.

857 Miall, A.D., 1977. A review of the braided river depositional environment. Earth-
858 Science Reviews 13, 1-62.

859 Miall, A.D., 1978. Lithofacies types and vertical profile models in braided river deposits:
860 a summary. In: Miall, A.D. (Ed.), Fluvial Sedimentology. Canadian Society of Petroleum
861 Geologists Memoir 5, pp. 597–604.

862 Montserrat-Martí, J.M., 1992. Evolución glaciar y postglaciar del clima y la vegetación
863 en la vertiente sur del Pirineo: Estudio palinológico. Monografías del IPE, Instituto
864 Pirenaico de Ecología (CSIC), Zaragoza, España, vol. 6, 147 pp.

865 Monserrat, J.M., Vilaplana, J.M., 1988. The paleoclimatic records of the Upper
866 Pleistocene and Holocene in the Llauset Valley (Central Pyrenees). Pirineos 129, 107-
867 113.

868 Mulder, T., Alexander, J., 2001. The physical character of subaqueous sedimentary
869 density flows and their deposits. Sedimentology 48, 269-299.

870 Muñoz, J.A., 2002. The Pyrenees. In: Gibbons, W, Moreno, T. (Eds.), The geology of
871 Spain. Geological Society, London, pp. 370-385.

872 Murray, A.S., Wintle, A.G., 2000. Luminiscence dating of quartz using an improved
873 single-aliquot regenerative-dose protocol. Radiation Measurements 32, 57-73.

874 Murray, A.S., Wintle, A.G., 2003. The single aliquot regenerative dose protocol:
875 potential for improvements in reliability. Radiation Measurements 37, 377-381.

876 Nussbaum, F., 1946. Orographische und morphologische untersuchungen in den
877 Ostlichen Pyrenäen. Jahresberichtr der Geographischen Gesellschaft von Bern XXV-
878 XXVI, 247 pp.

879 Palacios, D., Gómez-Ortiz, A., Andrés, N., Vázquez-Selem, L., Salvador-Franch, F., Oliva,
880 M., 2015. Maximum extent of Late Pleistocene glaciers and last deglaciation of La
881 Cerdanya mountains, Southeastern Pyrenees. Geomorphology 231, 116-129.

882 Palacios, D., Marcos, J., Vázquez-Selem, L., 2011. Last Glacial Maximum and
883 deglaciation of Sierra de Gredos, central Iberian Peninsula. Quaternary International
884 233, 16-26.

885 Pallás, R., Rodés, A., Braucher, R., Carcailler, J., Ortuño, M., Bordonau, J., Bourlés, D.,
886 Vilaplana, J.M., Masana, E., Santanach, P., 2006. Late Pleistocene and Holocene
887 glaciation in the Pyrenees: a critical review and new evidence from ^{10}Be exposure ages,
888 south-central Pyrenees. Quaternary Science Reviews 25, 2937-2963.

889 Pallás, R., Rodés, A., Braucher, R., Bourlès, D., Delmas, M., Calvet, M., Gunnell, Y.,
890 2010. Small, isolated glacial catchments as priority target for cosmogenic surface
891 dating of Pleistocene climate fluctuations, SE Pyrenees. Geology 38, 891-894.

892 Panzer, W., 1926. Talentwicklung und Eiszeitklima in nordöstlichen Spanien.
893 Abhandlungen der Senckenberg Naturforschung Gesellschaft 39, 141-182.

894 Penck, A., 1883. Die Eiszeit in der Pyrenaen. Mitt. Ver. Erdk. Leipzig. (Translated to
895 French: La période glaciaire dans les Pyrénées. Bulletin de la Société d'Histoire
896 Naturelle de Toulouse 19, 105-200.

897 Peña, J.L., Sancho, C., Lewis, C., McDonald, E., Rhodes, E., 2004. Datos cronológicos de
898 las morrenas terminales del glaciar del Gállego y su relación con las terrazas
899 fluvioglaciares (Pirineo de Huesca). In: Peña, J.L., Longares, L.A., Sánchez, M. (Eds.),
900 Geografía Física de Aragón: aspectos generales y temáticos. Universidad de Zaragoza -
901 Institución Fernando el Católico (CSIC), Zaragoza, España, pp. 71-84.

902 Pietras, J.T., Carrol, A.L., 2006. High-Resolution Stratigraphy of an Underfilled Lake
903 Basin: Wilkins Peak Member, Eocene Green River Formation, Wyoming, U.S.A. Journal
904 of Sedimentary Research 76, 1197–1214.

905 Prior, D.B., Bornhold, B.D., 1988. Submarine morphology and processes of fjord fan
906 deltas and related high gradient systems: modern examples from British Columbia. In:
907 Nemec, W., Steel, R.J. (Eds.), Fan Deltas: Sedimentology and Tectonic Settings.
908 Blackwell, London, pp. 125–143.

909 Rasmussen, S.O., Bigler, M., Blockley, S.P., Blunier, T., Buchardt, S.L., Clausen, H.B.,
910 Cvijanovic, I., Dahl-Jensen, D., Johnsen, S.J., Fischer, H., Gkinis, V., Guillevic, M., Hoek,
911 W.Z., Lowe, J.J., Pedro, J.B., Popp, T., Seierstad, I.K., Steffensen, J.P., Svensson, A.M.,
912 Vallelonga, P., Vinther, B.M., Walker, M.J.C., Wheatley, J.J., Winstrup, M., 2014. A
913 stratigraphic framework for abrupt climatic changes during the Last Glacial period
914 based on three synchronized Greenland ice-core records: refining and extending the
915 INTIMATE event stratigraphy. Quaternary Science Reviews 106, 14-28.

916 Reineck, H.E., Singh, I.B., 1980. Depositional sedimentary environments, second
917 edition. Springer-Verlag, Berlin Heidelberg, 549 pp.

918 Rhodes, E.J., 1988. Methodological considerations in the optical dating of quartz.
919 Quaternary Science Reviews 7, 395-400.

920 Rhodes, E.J., 2000. Observations of thermal transfer OSL signals in glacigenic quartz.
921 Radiation Measurements 32, 595-602.

922 Rhodes, E.J., Pownall, L., 1994. Zeroing of the OSL signal in quartz from young
923 glaciofluvial sediments. Radiation Measurements 23, 329-333.

924 Rhodes, E.J., Schwenninger, J.L., 2007. Dose rates and radioisotope concentrations in
925 the concrete calibration blocks at Oxford. Ancient TL 25, 5-8.

926 Ríos, L.M., Lanaja, J.M., Frutos, E., 1982. Mapa Geológico de España 1:50,000, hoja 178
927 (Broto). Instituto Geológico y Minero de España, Madrid, 60 pp.

928 Rodríguez-Rodríguez, L., Jiménez-Sánchez, M., Dominenguez-Cuesta, M.J.,
929 Rinterknecht, V., Pallàs, R., Bourlès, D., 2016. Chronology of glaciations in the
930 Cantabrian Mountains (NW Iberia) during the Last Glacial Cycle based on in situ-
931 produced ^{10}Be. Quaternary Science Reviews 138, 31-48.

932 Salgueiro, E., Voelker, A.H.L., de Abreu, L., Abrantes, F., Meggers, H., Wefer, G., 2010.
933 Temperature and productivity changes off the western Iberian margin during the last
934 150 ky. Quaternary Science Reviews 29, 680-695.

935 Sánchez-Goñi, M.F., Landais, A., Fletcher, W.J., Naughton, F., Desprat, S., Duprat, J.,
936 2008. Contrasting impacts of Dansgaard–Oeschger events over a western European
937 latitudinal transect modulated by orbital parameters. Quaternary Science Reviews 27,
938 1136-1151.

939 Sancho, C., Peña, J.L., Lewis, C., McDonald, E., Rhodes, E., 2003. Preliminary dating of
940 glacial and fluvial deposits in the Cinca River Valley (NE Spain): chronological evidences
941 for the Glacial Maximum in the Pyrenees? In: Ruiz, M.B., Dorado, M., Valdeolmillos, A.,
942 Gil, M.J., Bardají, T., Bustamante, I., Martínez, I. (Eds.), Quaternary climatic changes
943 and environmental crises in the Mediterranean region. Universidad de Alcalá-
944 Ministerio de Ciencia y Tecnología-INQUA, pp. 169-173.

945 Sancho, C., Peña, J.L., Lewis, C., McDonald, E., Rhodes, E., 2004. Registros fluviales y
946 glaciares cuaternarios en las cuencas de los ríos Cinca y Gállego (Pirineos y depresión
947 del Ebro). In: Colombo, F., Liesa, C.L., Meléndez, G., Pocoví, A., Sancho, C., Soria, A.R.

948 (Eds), Itinerarios Geológicos por Aragón. Geo-Guías 1, Sociedad Geológica de España,
949 pp. 181-205.

950 Sancho, C., Peña-Monné, J.L., Rhodes, E., Arenas, C., Pardo, G., García-Ruiz, J.M., Martí-
951 Bono, J.L., 2011. El registro glaciolacustre de Linás de Broto (Valle del Ara, Pirineo
952 central, Huesca): nuevas aportaciones. In: Turu, V., Constante, A. (Eds.), El Cuaternario
953 en España y áreas afines, avances en 2011. Resúmenes XIII Reunión Nacional de
954 Cuaternario, Andorra, pp. 11-14.

955 Sancho, C., Calle, M., Peña-Monné, J.L., Duval, M., Oliva-Urcia, B., Pueyo E.L., Benito,
956 G., Moreno, A., 2016. Dating the Earliest Pleistocene alluvial terrace of the Alcanadre
957 River (Ebro Basin, NE Spain): Insights into the landscape evolution and involved
958 processes. Quaternary International 407, 86-95.

959 Serrano, E., 1998. Geomorfología del Alto Gállego. Pirineo aragonés. Institución
960 Fernando El Católico (CSIC), Zaragoza, España, 501 pp.

961 Serrano, E., Martínez de Pisón, E., 1994. Geomorfología y evolución glaciar en el
962 Pirineo aragonés oriental. In: Martí-Bono, C., García-Ruiz, J.M. (Eds.), El glaciarismo
963 surpirenaico: nuevas aportaciones. Geoforma Ediciones, Logroño, España, pp. 33-64.

964 Serrat, D., Vilaplana, J.M., Martí-Bono, C., 1982. Some depositional models in
965 glaciolacustrine environments (southern Pyrenees). In: Evenson, E.B., Schlüchter, Ch.,
966 Rabassa, J. (Eds.), Tills and related deposits. Balkema, Rotterdam, pp. 231-244.

967 Shulmeister, J., Thackray, G.D., Rieser, U., Hyatt, O.M. Rother, H., Smart, C.C., Evans,
968 D.J.A., 2010. The stratigraphy, timing and climatic implications of glaciolacustrine

969 deposits in the middle Rakaia Valley, South Island, New Zealand. Quaternary Science
970 Reviews 29, 2362-2381.

971 Smith, L.N., 2017. Repeated sedimentation and exposure of glacial Lake Missoula
972 sediments: A lake-level history at Garden Gulch, Montana, USA. Quaternary Science
973 Reviews 155, 114-126.

974 Stanley, K.O., 1974. Morphology and hydraulic significance of climbing ripples with
975 superimposed micro-ripple-drift cross-lamination in Lower Quaternary lake silts,
976 Nebraska. Journal of Sedimentary Petrology 44, 472-483.

977 Turu, V., 2002. Análisis secuencial del delta de Erts. Estratigrafía de un valle glaciar
978 obturado intermitentemente, relación con el último ciclo glaciar. Valle de Arinsal,
979 Pirineos Orientales. In: Estudios recientes (2000-2002) en geomorfología, patrimonio,
980 montaña y dinámica territorial. Sociedad Española de Geomorfología-Universidad de
981 Valladolid, España, pp. 565-574.

982 Turu, V., Calvet, M., Bordonau, J., Gunnell, Y., Delmas, M., Vilaplana, J.M., Jalut, G.,
983 2017. Did Pyrenean glaciers dance to the beat of global climatic events? Evidence from
984 the Würmian sequence stratigraphy of an ice-dammed paleolake depocentre in
985 Andorra. In: Hughes, P.D., Woodward, J.C. (Eds.), Quaternary glaciation in the
986 Mediterranean mountains. Geological Society of London, Special Publications 433, pp.
987 111-136.

988 Vera, J.A. (Ed.), 2004. Geología de España. Sociedad Geológica de España-Instituto
989 Geológico y Minero de España, Madrid, 890 pp.

990 Vilaplana, J.M., 1983. Estudi del glaciarisme quaternari de les altes valls de la
991 Ribagorça. PhD Thesis. Universitat de Barcelona, 322 pp.

992 Vilaplana, J.M., Monserrat, J., Schluchter, Ch., 1989. Recent progress in Quaternary
993 stratigraphy: the Lake Llauset sequences in the Spanish Pyrenees. In: Rose, J.,
994 Schluchter, Ch. (Eds.), Quaternary type sections: imagination or reality? Balkema,
995 Rotterdam, pp. 123-134.

996 Vilaplana, J.M., Schluchter, Ch., Verdaguer, A., 1983. Sedimentology and stratigraphy
997 of the Pleistocene sediments in Lake Llauser (Southern Pyrenees, Spain). A first
998 approach. Acta Geológica Hispánica 18, 235-248.

999 Waelbroeck, C., Kiefer, T., Dokken, T., Chen, M.-T., Spero, H.J., Jung, S., Veinelt, M.,
1000 Kucera, M., Paul, A. on behalf of MARGO Project Members, 2014. Constraints on
1001 surface seawater oxygen isotope change between the Last Glacial Maximum and the
1002 Late Holocene. Quaternary Science Reviews 105, 102-111.

1003 Wang, X., Vanderberghe, J., Shuangwen, Y., Van Balen, R., Lu, H., 2015. Climate-
1004 dependent fluvial architecture and processes on a suborbital timescale in areas of
1005 rapid tectonic uplift: An example from the NE Tibetan Plateau. Global and Planetary
1006 Change 133, 318-329.

1007 Winsemann, J., Asprion, U., Meyer, T., 2007. Facies characteristics of Middle
1008 Pleistocene (Saalian) ice-margin subaqueous fan and delta deposits, glacial Lake Leine,
1009 NW Germany. Sedimentary Geology 193, 105–129.

1010

FIGURE AND TABLE CAPTIONS

Figure 1. (A) Location of the studied area. (B) Geologic setting adapted from Mapa Geológico de España, 1:2,000,000 (Vera, 2004). Sites with Pleistocene glacial and fluvial records relevant to this study: 1a: River Aragón (Castiello de Jaca, terrace; García Ruiz et al., 2013); 1b: River Aragón (Castiello de Jaca, moraine; García Ruiz et al., 2013). 2a: River Gállego (Senegüé, moraine; Lewis et al., 2009); 2b: River Gállego (Sabiñánigo, fluvio-glacial terrace; Lewis et al., 2009); 2c: River Gállego (Murillo de Gállego, terrace; Lewis et al., 2009). 3: River Ara (Asín de Broto, moraine; Serrano and Martínez de Pisón, 1994). 4a: River Cinca (Salinas de Sin, moraine; Sancho et al. 2003, 2004; Lewis et al., 2009); 4b: River Cinca (El Grado, terrace Qt8; Lewis et al., 2009); 4c: River Cinca (Alfántega, terrace Qt7; Lewis et al., 2009). 5: River Valira (Andorra, moraines; Turu et al., 2017). 6: Ariège valley (northeastern Pyerenees, France, moraines; Delmas et al., 2011).

Figure 2. (A) Geomorphologic map of the studied area. Sorrosal glacier moraines: S1, S2 and S3. (B) Detailed map of the Linás de Broto area, with location of stratigraphic sections LB1 and LB2. In A and B, Ara glacier moraine at Viu: A1.a, A1.b and A.1c. A.1c is a kame terrace (with no morphological expression at map scale); Ara glacier moraine at Fragen: A2. (C) Reconstruction of the maximum glacier extension of the Ara glacier during the Last Glacial Cycle (based on Serrano and Martínez de Pisón, 1994; Martí-Bono, 1996).

Figure 3. Stratigraphic sections measured in the River Sorrosal valley (location in figure 2B). Section LB1 is adapted from Sancho et al. (2011). Correlation is based on physical

1033 continuity of sedimentary surfaces (e.g., gravel beds) in the field. Facies nomenclature
1034 in Table 1 and facies associations in Figure 10.

1035 Figure 4. (A) Panoramic view of the Linás de Broto outcrop, with location of the two
1036 stratigraphic sections and correlation of units based on continuity of sedimentary
1037 surfaces and lithological composition. (B) Field image that shows a portion of Unit 1,
1038 with the lowermost sand and gravel outcrop.

1039 Figure 5. Field views of sedimentary facies (gravels) and facies associations. See Table 1
1040 for nomenclature and features of facies and Figure 10 for facies associations. (A, B)
1041 Structureless (Gm) and horizontal-stratified (Gh) clast-supported gravels and
1042 horizontal-laminated sands (Sh), arranged as FA 1. (C) Detail of structureless clast-
1043 supported gravels (Gm), with rip-up clasts (arrowed) and interbedded thin sand
1044 interval (facies Sh). (D) Structureless sandy-rich, clast-supported gravels (Gm, in FA
1045 1B). (E) Erratic clast (≈ 0.5 m long) in Unit 1. (F) Foreset cross-stratification in gravels
1046 (Gf) and sands (Sf) in FA 2A, and overlying structureless clast-supported gravels. (G)
1047 Detail of foreset cross-stratification, underlying sands with ripples (facies Sr2) and
1048 horizontal lamination (facies Sh). (H) Detail of gravel and sand wedges at the distal
1049 termination of foresets in facies Gf and Sf.

1050 Figure 6. Field views of sedimentary facies (sand and silt) and facies associations. See
1051 Table 1 for nomenclature and features of facies and Figure 10 for facies associations.
1052 (A) Sands of Unit 2, structureless (facies Sm), with horizontal lamination (Sh) and in-
1053 phase climbling ripple lamination (Sr1) (FA 2A), underlying structureless gravels (Gm)
1054 of Unit 3. (B) In-phase and in-drift climbling ripple lamination (Sr1) in sands of Unit 2.

(C) In-drift climbing ripple lamination (Sr1) in sands of Unit 2. (D) In-drift climbing ripple lamination (Sr1) and structureless (Sm) sands of Unit 2. (E) Sands with horizontal lamination (Sh) and scour and fill (Ss) stratification, underlying cross-stratified sands and gravels (St, Gt), forming FA 2C. (Unit 2). (F) Foreset cross-stratification in sands and minor gravels (Sf, Gf), overlying sands with horizontal and ripple lamination (Sh, Sr1 and Sr2) of Unit 1 (section LB-1), arranged as FA 2A. Note overlying structureless gravels of Unit 3. (G) Assymmetric ripples (Sr2) and structureless sand with erratics (Sm) at the base of a coarsening upward sequence (FA 2A) underlying Unit 1.

Figure 7. Field views of sedimentary facies (silt and clay) and lacustrine facies associations. See Table 1 for nomenclature and features of facies and Figure 10 for facies associations. (A) Ripple cross-laminated silts (Fr), horizontal-laminated sand (Sh) and gravel (Gh), and structureless gravel (Gm), arranged in a coarsening upward sequence (FA 3A). (B) Alternating structureless gravel (Gm) and laminated and structureless clays (Clh, Clm) forming FA 4A. (C) Structureless and horizontal-laminated silts (Fm, Fh) and clays (Clh) forming FA 4B. (D) Alternating structureless silts and sands (Fm, Sm) and horizontal-laminated clays (Clh), representing FA 6A. (E) Alternating structureless silts and clays (Fm, Clm) and horizontal-laminated clays (Clh), representing FA 6B. (F) Detail of structureless and laminated clays containing dropstones (FA 6B).

Figure 8. Photomicrographs (A, B, D, optical microscope; C, scanning electron microscope, SEM) of horizontal-laminated mudstones that consist of clay laminae and thin silt interlaminae and interlenses (facies Clh). (A , B) Sharp basal contacts and fining upward as far as the following silt interval. (C) Detail of fining-upward evolution of a

lamina (C: calcite; Q: quartz). (D) Dropstones, and deformed and undulate laminae. (A to D), the coarser grains are of quartz, calcite, and minor dolomite, rutile, apatite, iron oxides and pyrite; the finest particles mostly correspond to chlorite/clinochlore and muscovite (determined by XRD analysis and SEM microanalyses).

Figure 9. Field views of deformation structures. (A) Irregular folds in sand and gravel beds of Units 1 and 2. (B) Acute folds in sand beds of Unit 2. (C) Clay injections (flames) within fine sand bed (arrow at the bottom) and micrograben in horizontal-laminated sands bed (arrows). (D) Gently deformed lamination in clays and silts. (E, F) Clay injections (mushroom-shaped, cream and pale yellow in colour; arrows) within silt and fine sand laminated layers of Unit 2.

Figure 10. Facies associations formed in fluvial, deltaic and lacustrine environments. Explanation in the text. Nomenclature and summary of main features of the sedimentary facies are given in Table 1.

Figure 11. Sedimentary facies model for an ice-dammed lake (trunk glacier-valley ponded lake) that receives sediment supply through an outwash train fed by meltwater from a small glacier developed in the headwater of the tributary River Sorrosal valley. (A) Expansion of the lake, illustrated by stage 2 (as an example of the depositional settings of Units 2 and 4). (B) Progradation of fluvial streams and reduction of the lake during warmer periods, with outflow through former moraine dam, illustrated by stage 3 (as an example of the depositional settings of Units 1, 3 and 5).

1099 Figure 12. Two main stages of development of the glaciofluvial and glaciolacustrine
1100 system in the Linás de Broto ice-dammed lake: (A) Progradation of the braided fluvial
1101 system during warmer conditions, with reduction (or final disappearance) of lake
1102 surface (Units 1, 3 and 5). (B) Expansion of the lake due to closure by moraine and ice
1103 growth of the trunk glacier, with retrogradation of the fluvial braided system, during
1104 colder conditions (Units 2 and 4).

1105 Table 1. Sedimentary facies and their interpretation in the Pleistocene deposits studied
1106 at Linás de Broto area.

1107 Table 2. Optically Stimulated Luminiscence (OSL) dates from glacial and
1108 glaciolacustrine deposits on the River Sorrosal valley (adapted from Sancho et al.,
1109 2011). Location of glaciolacustrine dated samples is shown in figure 3 (LB1
1110 stratigraphic section). Depth refers to thickness downward from the top of section
1111 (i.e., outcropping deposit).

1112 Table 3. Summary of ages obtained in the studied Sorrosal valley and in Pleistocene
1113 glacial and fluvial records relevant to this study in the northeastern Iberian Peninsula.
1114 Location of points and correspondent authors in Fig. 1B.

Figure 01

Click here to download high resolution image

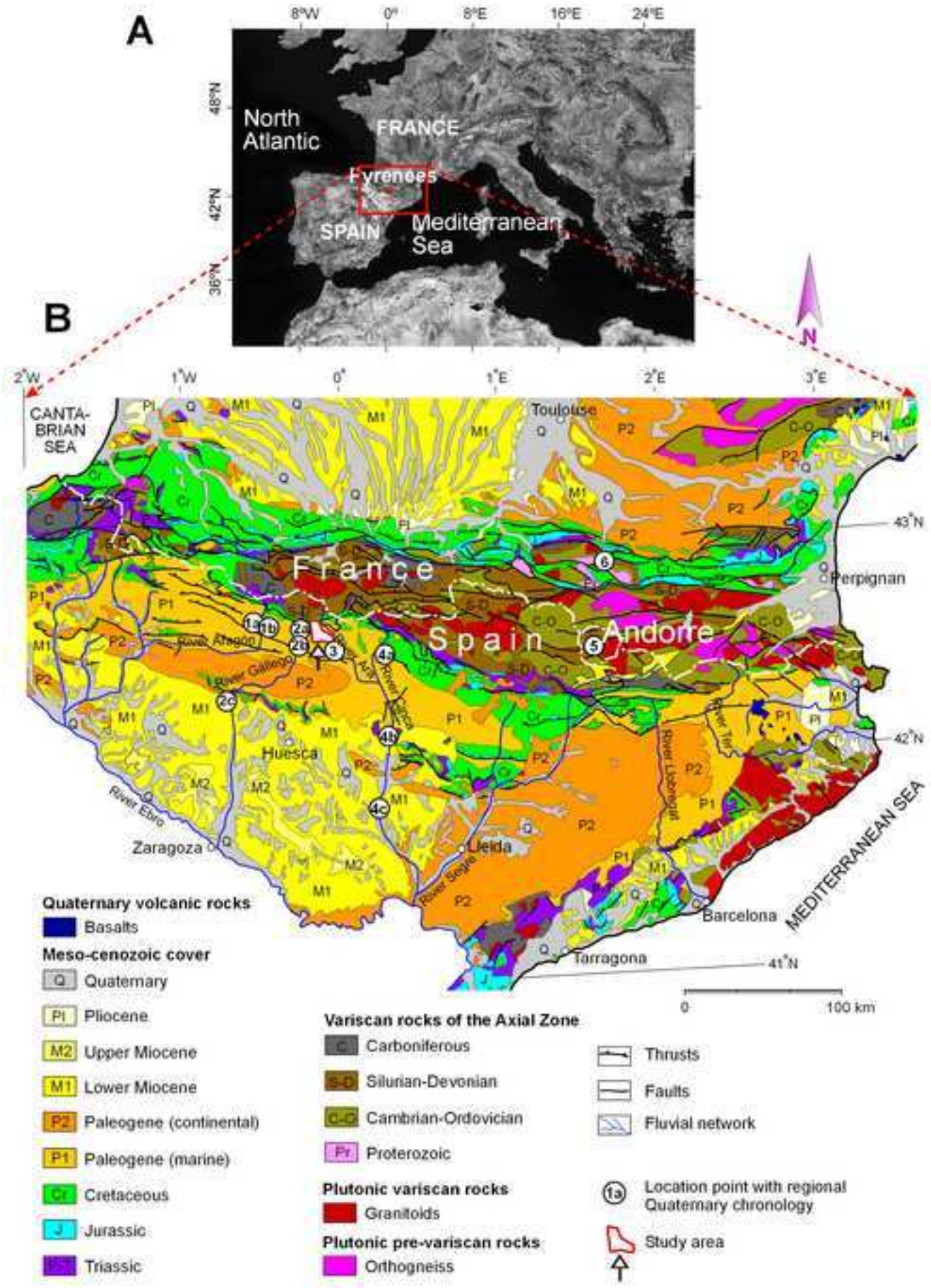

Figure 02

Click here to download high resolution image

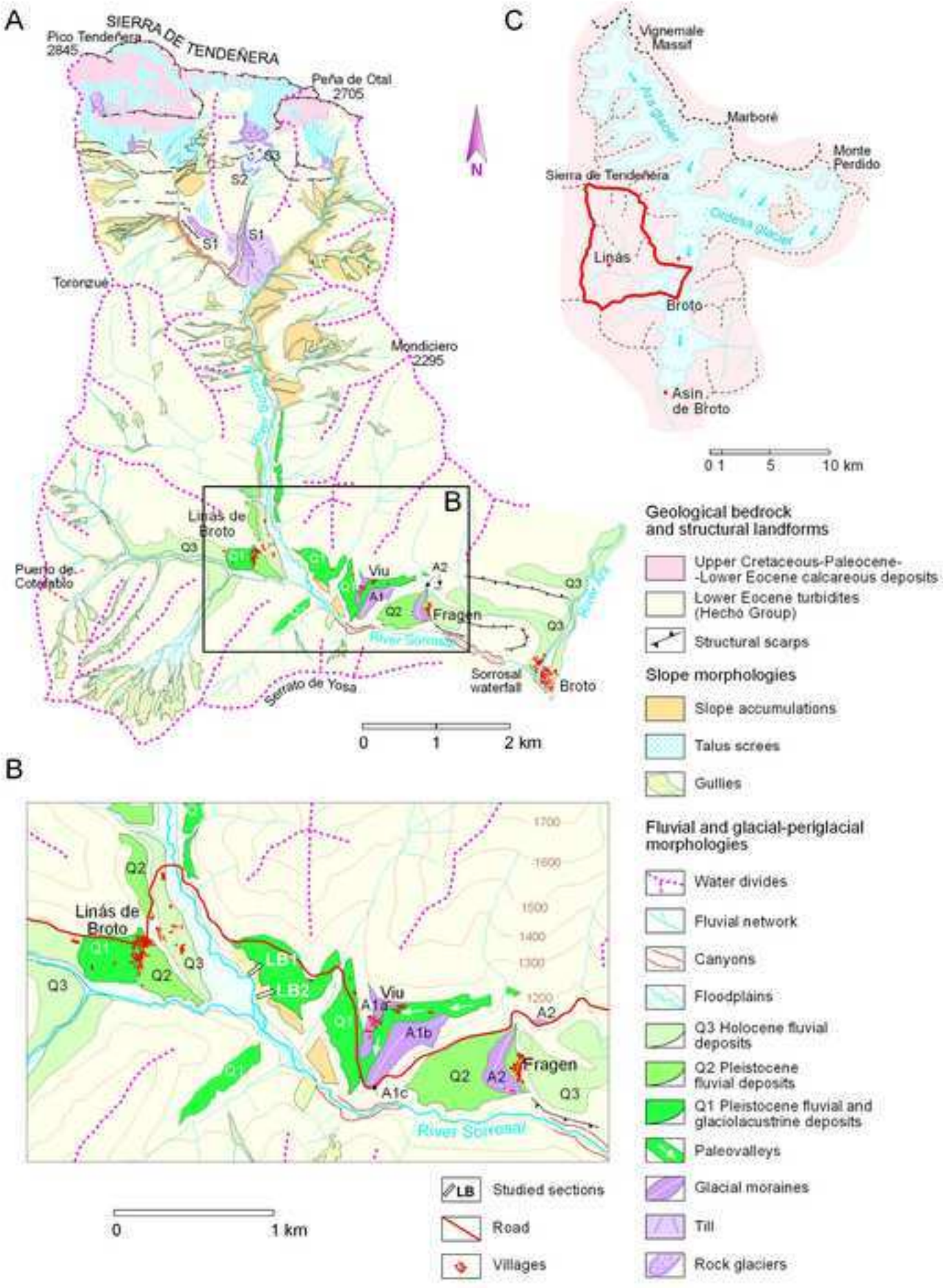

Figure 03

Click here to download high resolution image

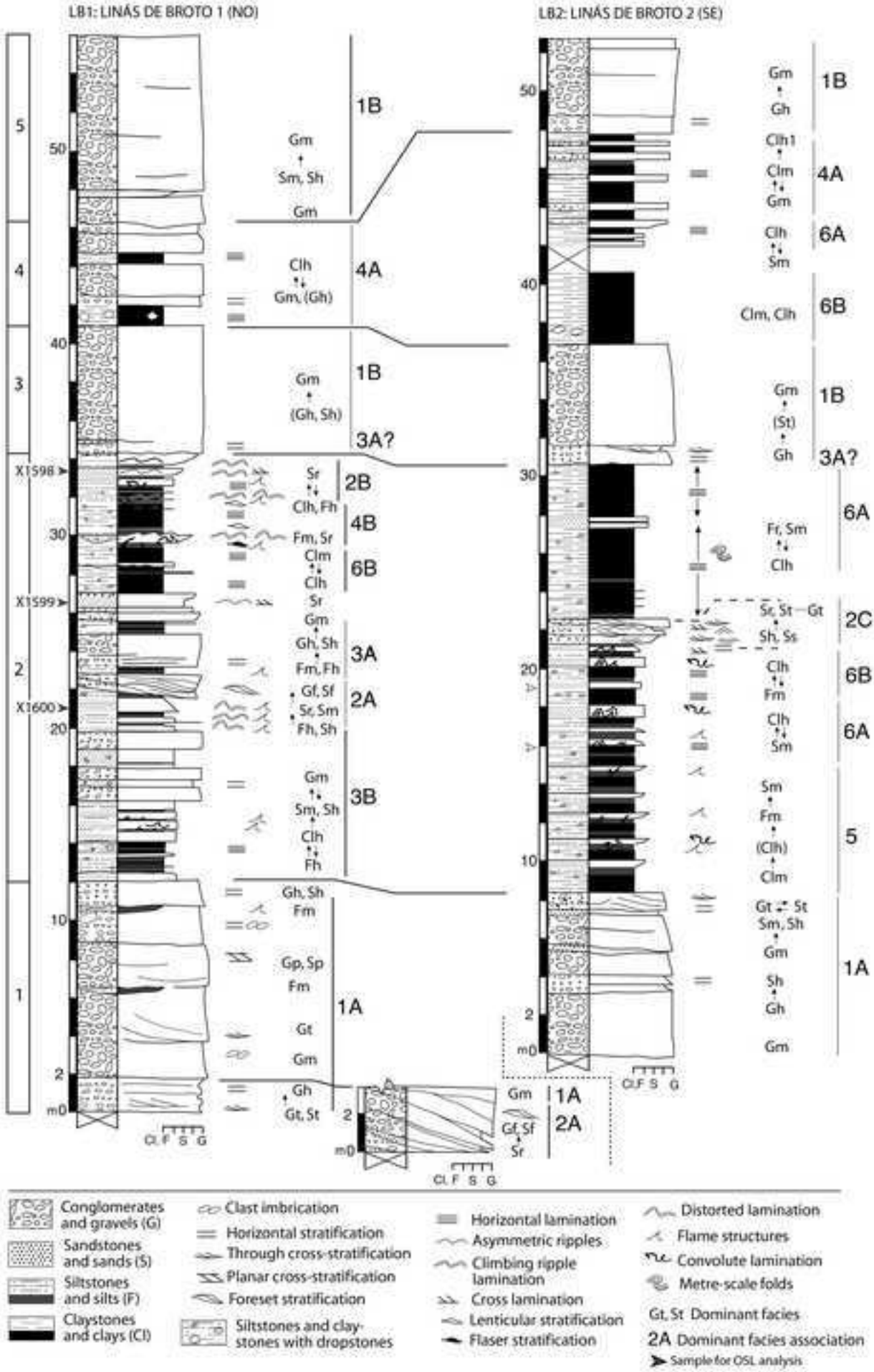

Figure 04

Click here to download high resolution image

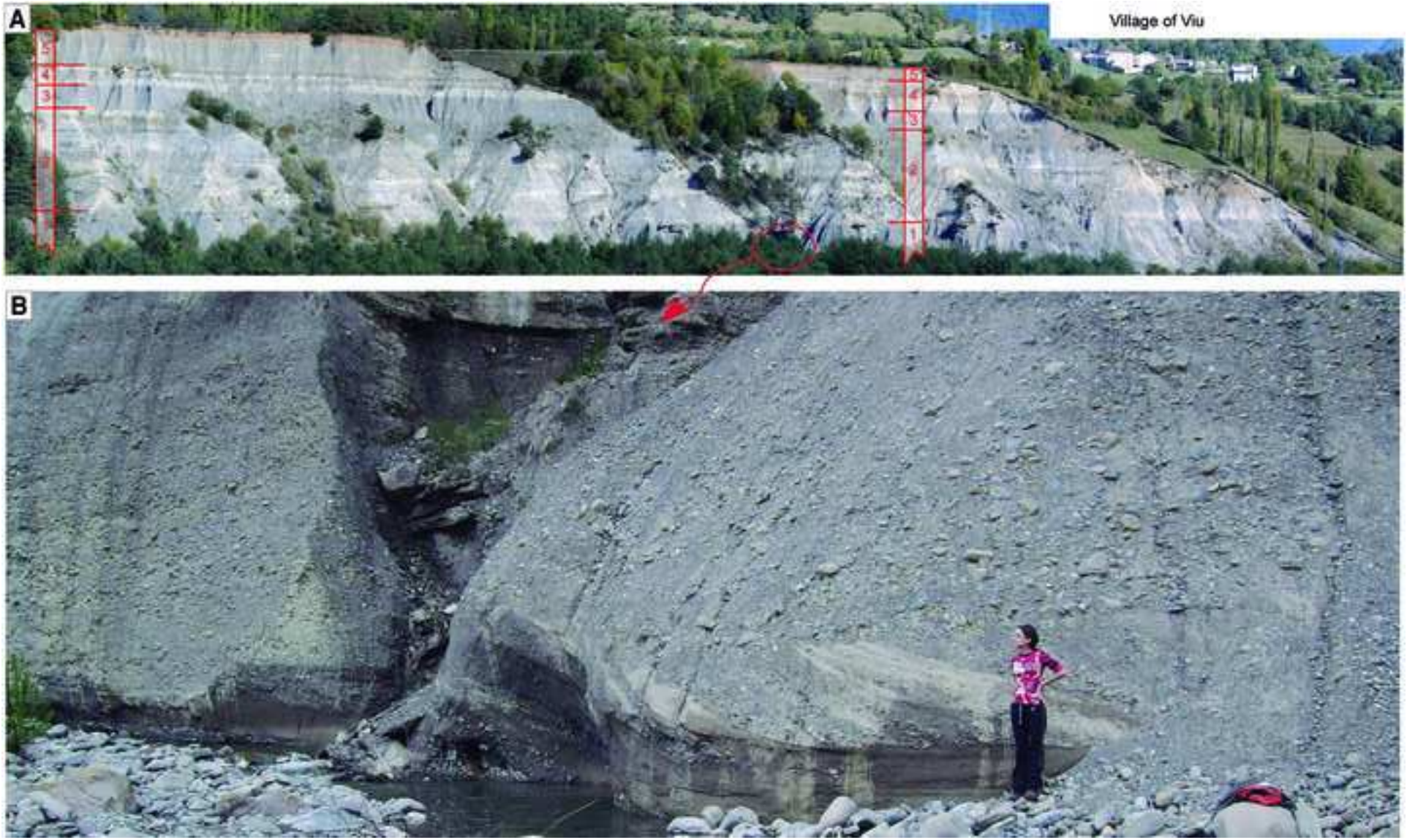

Figure 05

Click here to download high resolution image

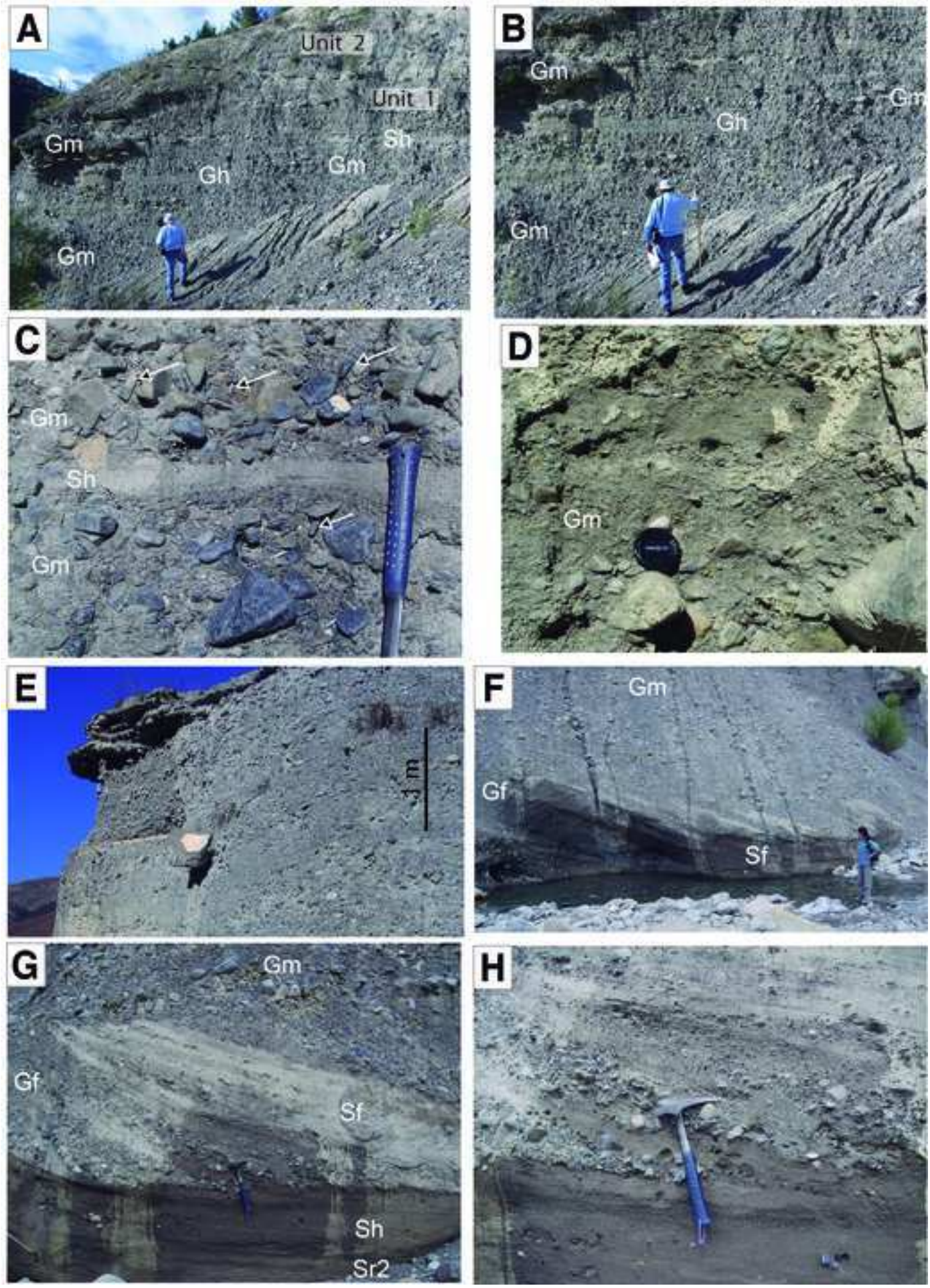

Figure 06
Click here to download high resolution image

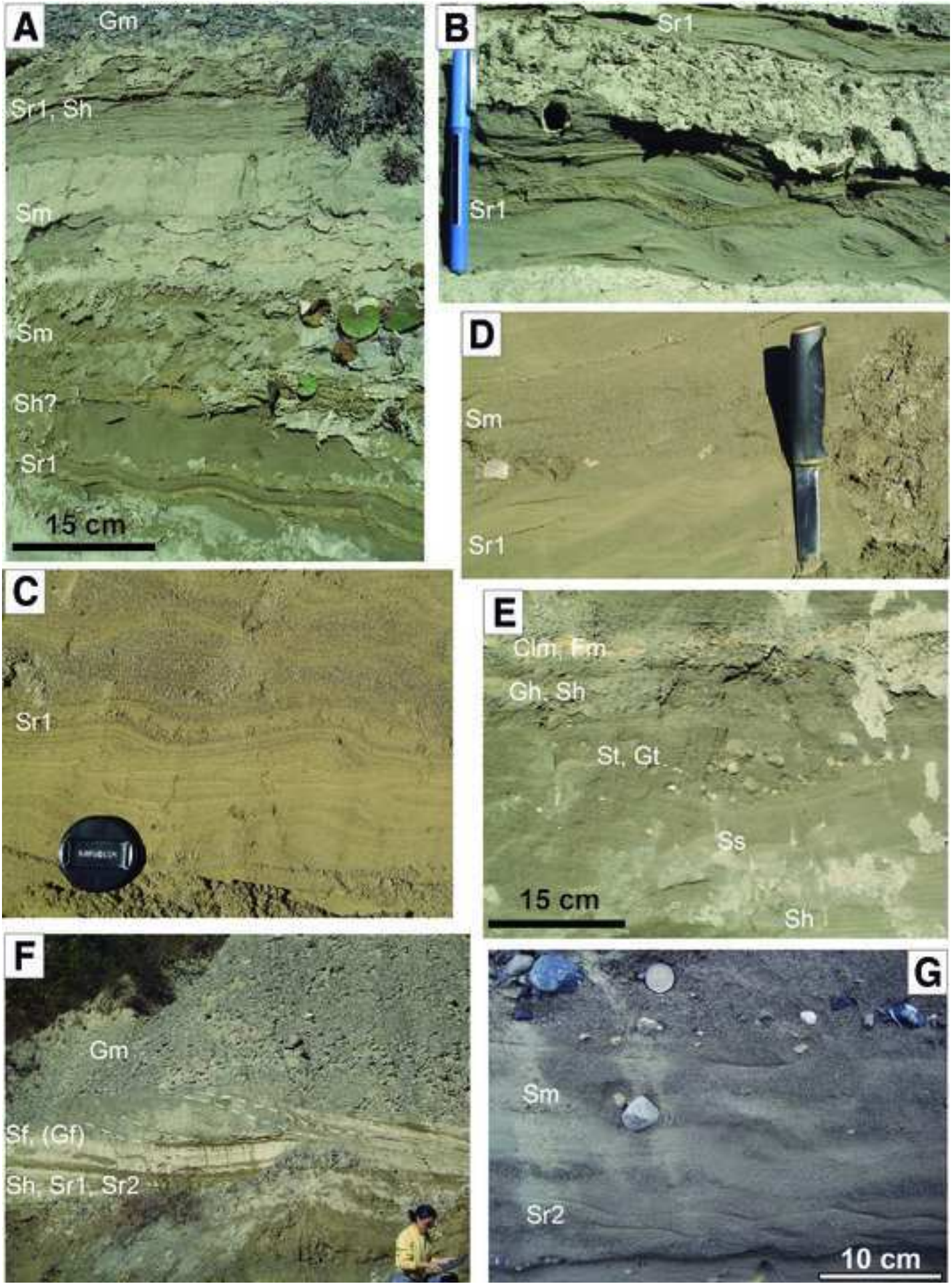

Figure 07

Click here to download high resolution image

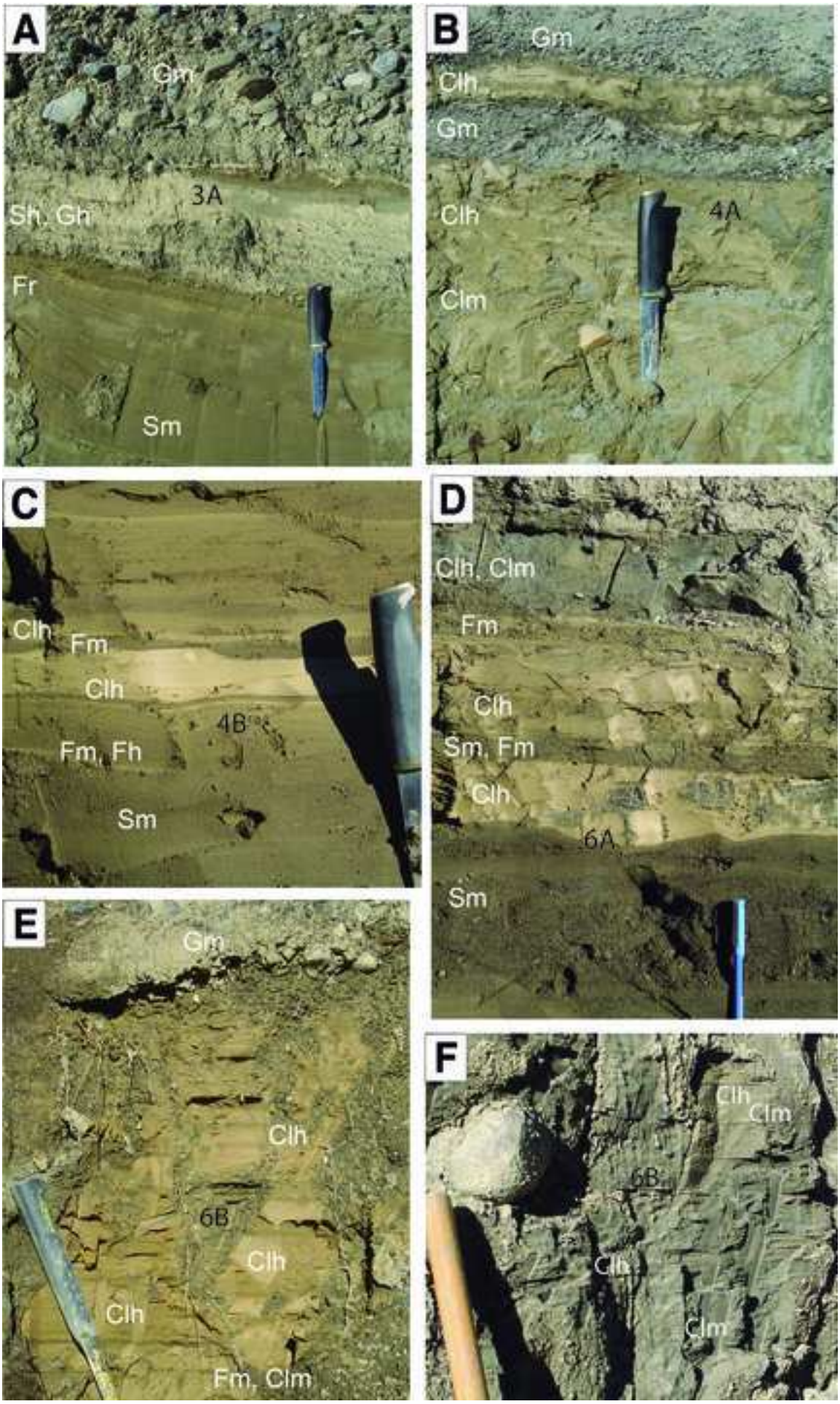

Figure 08
Click here to download high resolution image

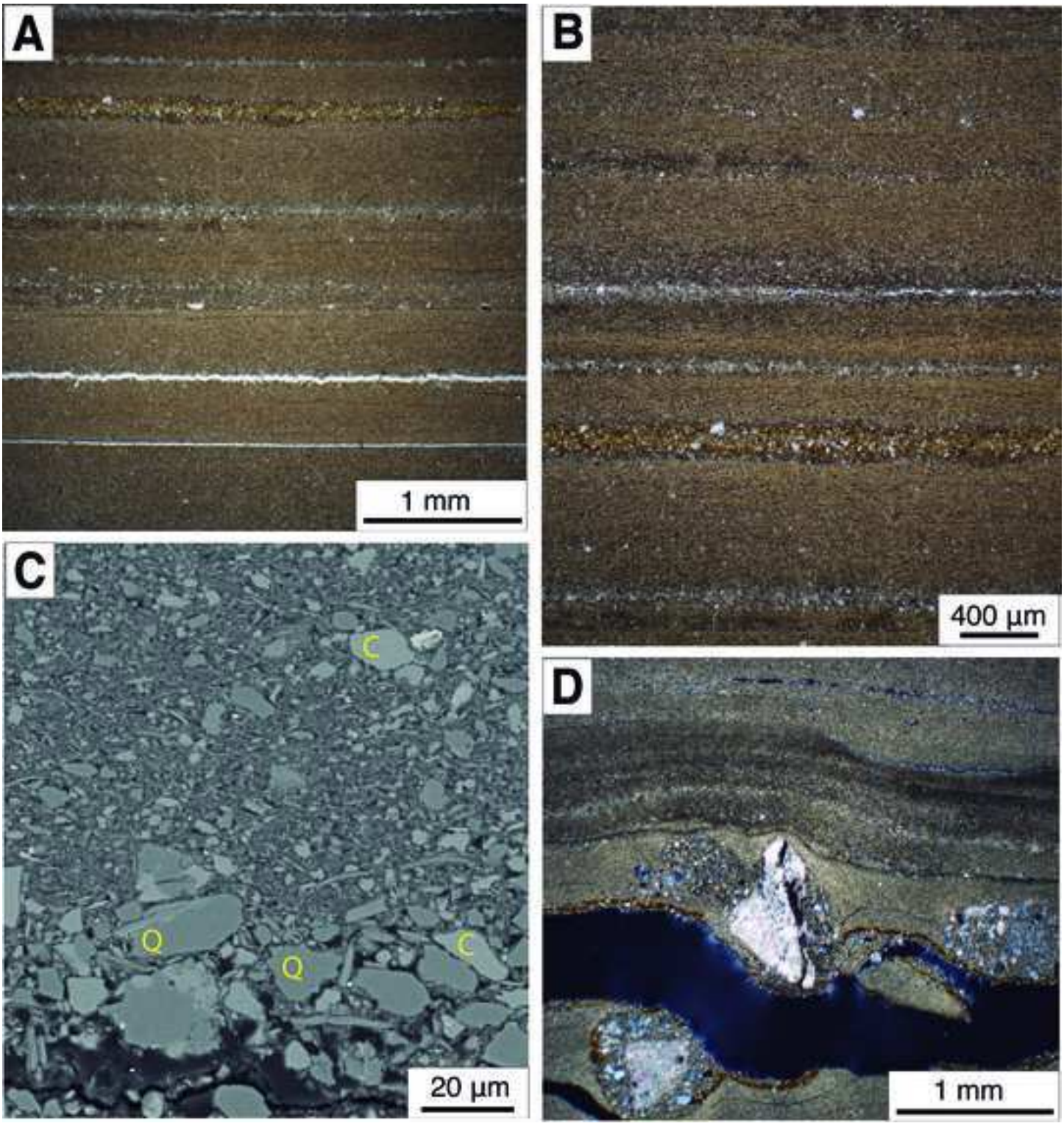

Figure 09

Click here to download high resolution image

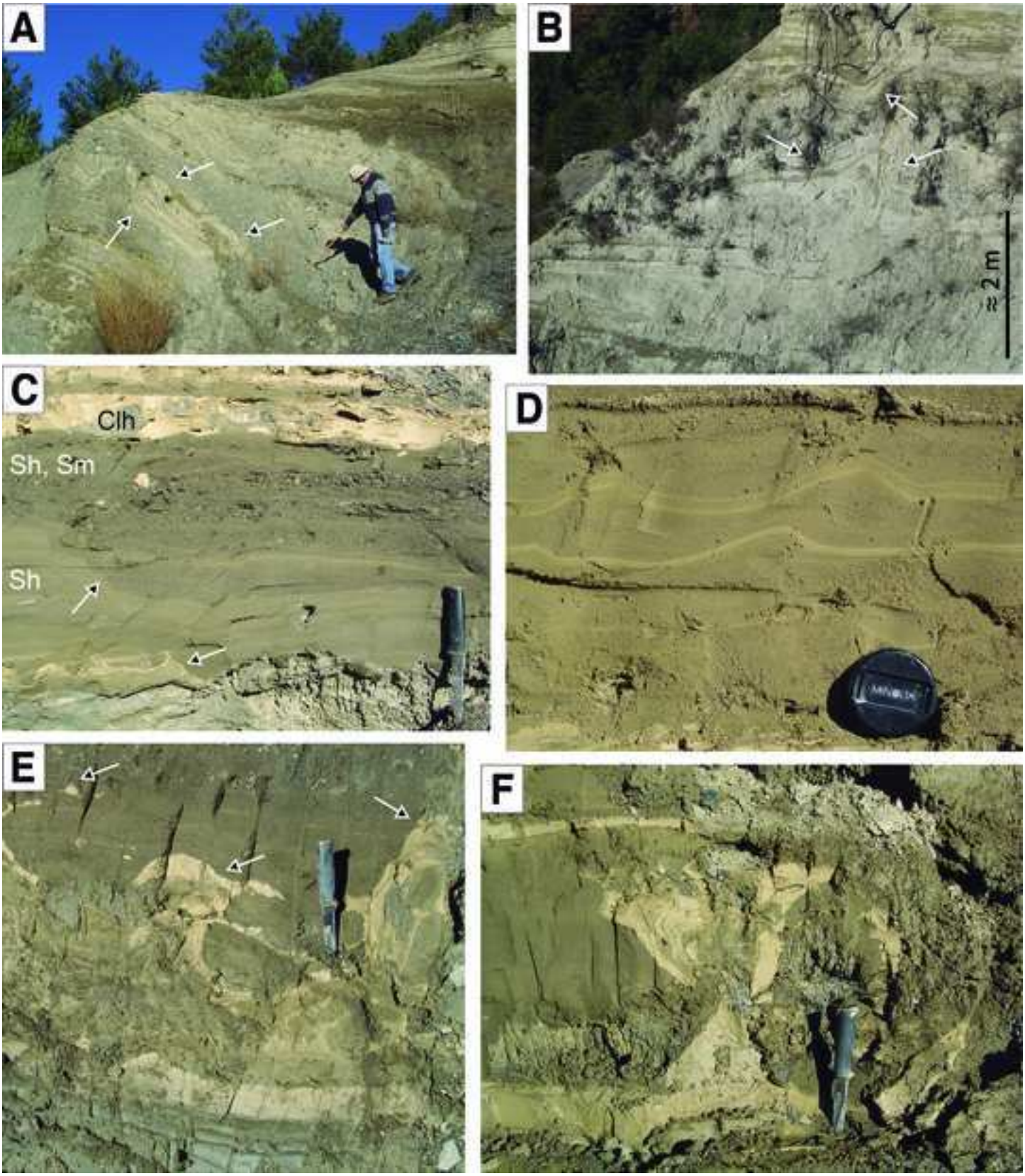

Figure 10

Click here to download high resolution image

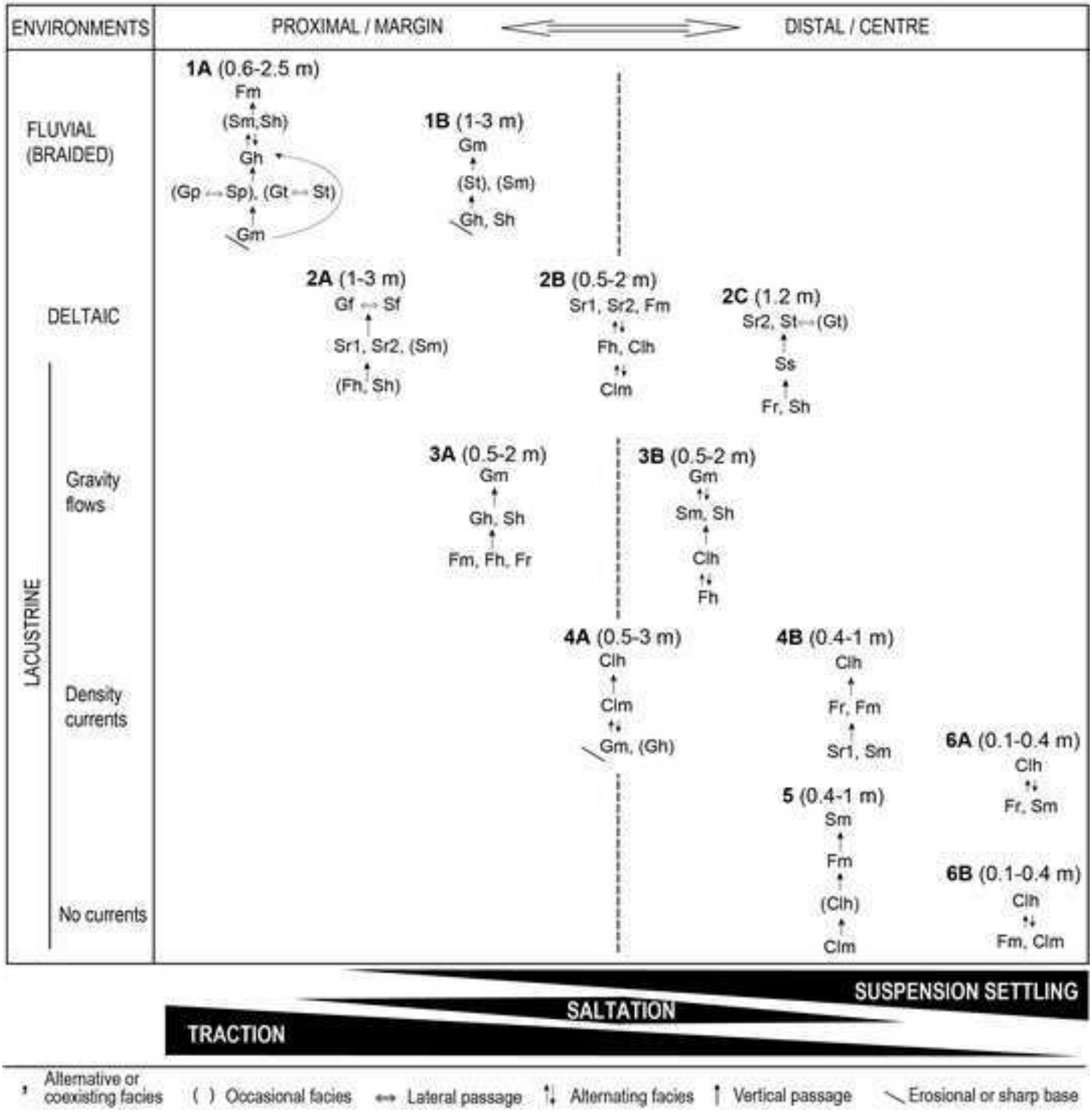

Figure 11

Click here to download high resolution image

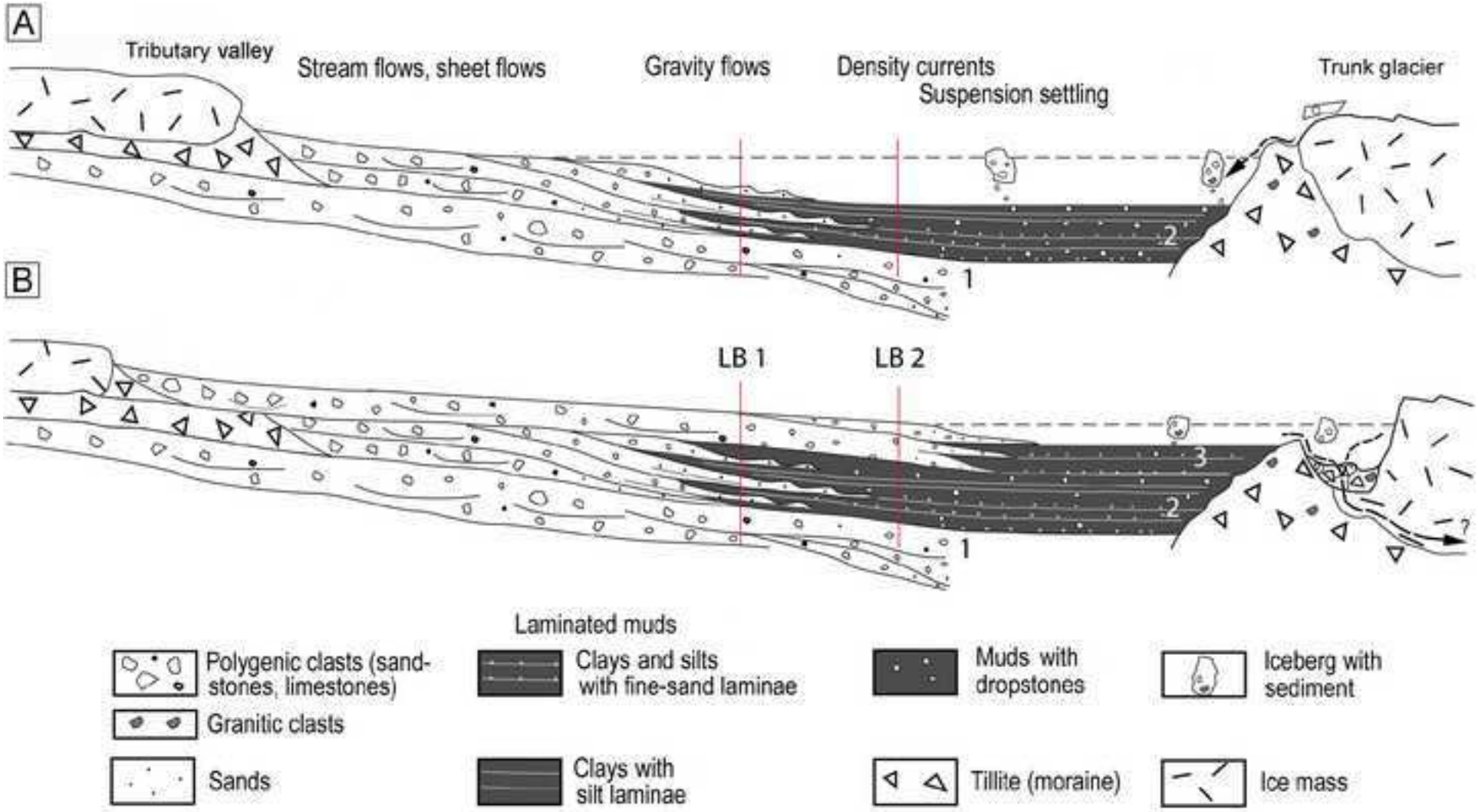

Figure 12

Click here to download high resolution image

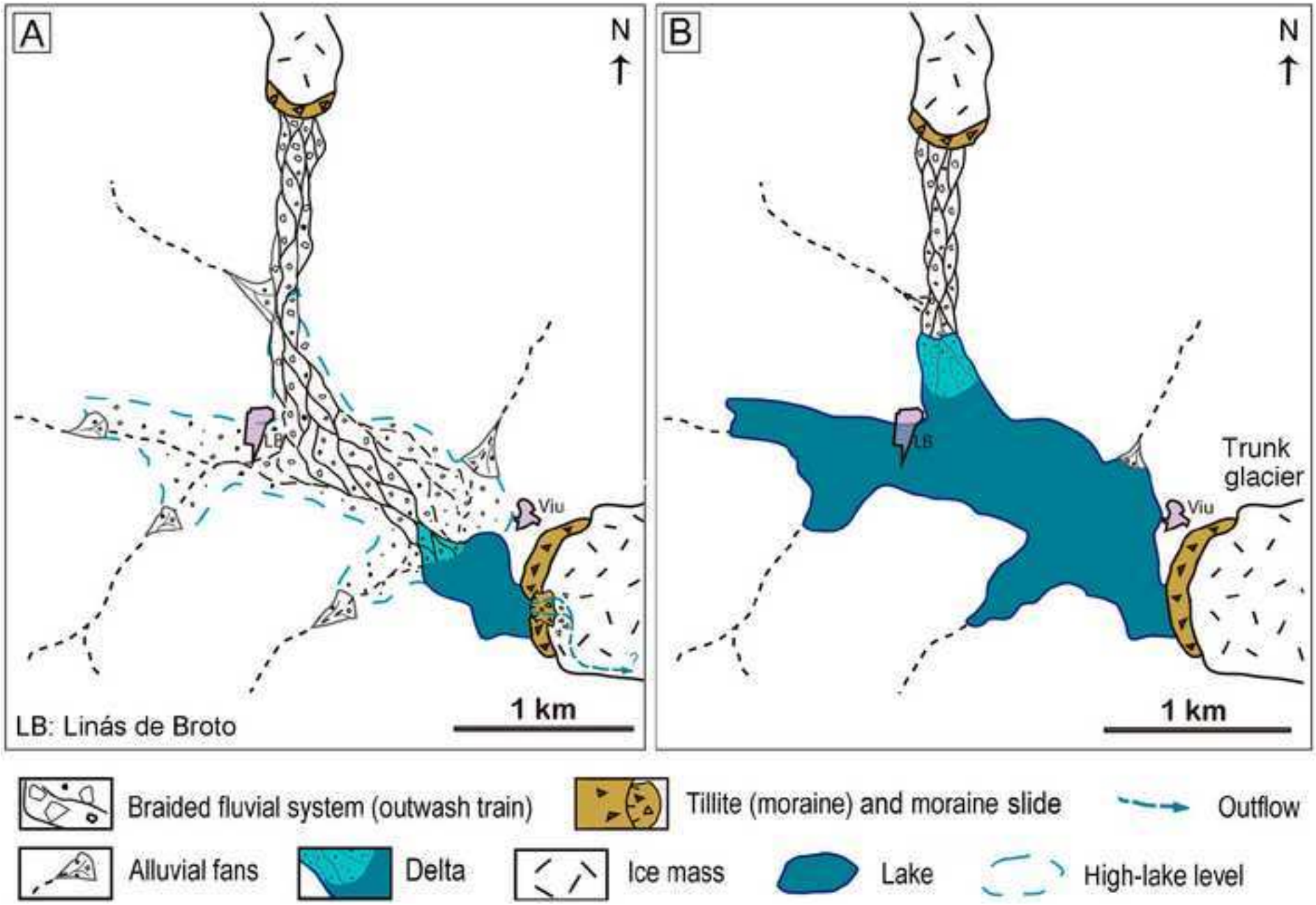

Table01

Click here to download Table: Table01R1.doc

Lithology	Texture and geometry of deposits	Sedimentary Facies	Interpretation: processes and depositional settings
Gravels. Figs. 4B, 5, 6F, 7A.	Grey to brown in colour. Clast-supported fabric. Polymictic clasts, mostly of brown to grey sandstones and dark grey limestones (from Palaeocene-Illerdian units and Eocene Hecho Group), and very rare granite clasts; commonly heterometric, from a few cm to 35 cm, apart from erractics than can reach up to 1.2 m in length; varied in shape and from poorly rounded to subrounded. Granule and sand matrix and very minor calcareous cement.	**Gm**: structureless, with rip-up clasts, fining-upward, coarsening upward or without size vertical trend. Figs. 4B, 5A, 5B, 5C, 5D, 5E.	Gm: Flash flood deposits and bar cores in braided fluvial context (Miall, 1978, 2000; Arenas et al., 1989). Deposition from a high-velocity expanding jet onshore and offshore (Ashley, 2002).
		Gh: horizontal stratification, with or without clast imbrication. Folds. Figs. 5A, B, E, 9A.	Deposition in longitudinal bars of braided fluvial systems (Gh<> Sh) (Miall, 1978; Arenas et al., 1989).
		Gp: planar cross-stratification, sets dm thick. **Gt:** through cross-tratification, sets dm thick.	Deposition in transverse bars and crescent dunes in shallow braided channels (Miall, 1978, 2000).
	Generally thick, up to 3 m, tabular bodies with crude stratification, and planar or wide concave bases. Locally, wedge- and lense-shaped bodies up to 1 m thick.	**Gf:** foreset cross-stratification. Wedge- and lense-shaped (sigmoid) bodies dm thick. Figs. 4B, 5F, 5G, 5H.	Deltaic foresets on lacustrine margins (Kostic et al., 2005; Winsemann et al., 2007).
Sands (commonly associated with thin layers of silt or mud). Figs. 6, 7A, 7C, 7D.	Grey, yellow and light brown, very coarse to fine particle sand size; polymictic grains; with or without calcareous cement.	**Sm:** structureless or with contorted laminae and flames from underlying silt and clay layers. Microfaults. Figs. 6A, 6D, 6G, 7A, 7C, 7D, 9C.	Deposition from a high-velocity expanding flow (Ashley, 2002).
	Generally tabular, with planar or slightly concave bases, and locally lenticular (channel-like). Internal concave surfaces. Up to 1 m thick.	**St**: trough cross-stratification, sets dm thick. **Sp**: planar cross-stratification, sets dm thick.	Deposition in shallow braided fluvial systems, frequently as channel fills (St<> Gt; Sp<>Gp) (Miall, 1978; Allen, 1982).
		Ss: scour and fills, dm thick. Fig. 6E.	Scour and fill in high-velocity flow conditions.
		Sh: horizontal lamination; clay flames and convoluted laminae. Figs. 6A, 6E, 9B, 9C, 9E,	Traction from turbidite flows (Allen, 1982; Johnsen and Brennand, 2006). Lacustrine deposition from

		9F.	successive high-velocity expanding sheet flows in prodelta and distal areas (Blair, 1987).
		Sr1: with ripple lamination and climbing ripples, mostly of type B (with stoss and lee laminae), with mud drapes. Contorted laminae. Figs. 6A to 6D, 9D. **Sr2**: with small scale cross lamination, current ripples. Figs. 5G, 6G.	Sr, and associated Sh: Traction and suspension from turbitity currents forming ripples and laminae in delta foresets, prodelta and distal lake areas (Mulder and Alexander, 2001; Johnsen and Brennand, 2006 and references therein). Sr1: high deposition rates. Soft sediment deformation
		Sf: foreset cross-stratification. Sigmoid- and lense-shaped bodies dm thick. Fig. 6F.	Deltaic foresets on lake margins (Arenas et al., 1989; Winsemann et al., 2007), commonly associated with Sf.
Silts. In many cases, alternating with or interbedded within fine sands and/or clays. Figs. 7A, 7B, 7C, 8A, 8B	Yellow to light brown. Tabular deposits up to 2 m thick, consisting of single bodies 1 to 15 cm thick. Common dropstones mm to cm long.	**Fm:** structuress or with fine-sand flames and contorted laminae. Fig. 7C, D, E. **Fr**: climbing ripple lamination (type B) and lenticular stratification. Fig. 7A. **Fh**: horizontal lamination and layering (silt layers 2-3 cm thick). Figs. 7C, 8A, 8B.	Lacustrine deposition in prodelta and distal lake area. Traction current activity (Evans et al., 2013) and, for Fh and Fm, also suspension settling. Iceberg-rafting of dropstones.
Clays. In some cases, including mm to sub-mm silt laminae. Figs. 7B to 7F, 8.	Grey, green and ochre. Yellow to beige. Tabular deposits up to 4.5 m thick, commonly consisting of tabular layers 2 to 15 cm thick distinguished by colour. Common dropstones mm to ca. 1 m long.	**Clm**: structureless. At places with folding (slumps). Fig. 7B, D, E, F. **Clh:** horizontal lamination; very thin (mm to sub-mm thick) rythmic laminae that are grouped in layers up to 15 cm thick. At places with folding (slumps). Figs. 7B to 7F, 8A to 8D.	Offshore (distal lake area), uniform (Clm) or rhythmic deposition (Clh), mainly from suspension settling. Iceberg-rafting of dropstones (Ashley, 2002; Johnsen and Brennand, 2006; Evans et al., 2013).

Table 2. Lithofacies and their characteristics in the studied area to the east of Linás de Broto. Lithofacies Nomenclature and abreviation adapted to the study case from Miall (1978)'s code.

Table 02

Click here to download Table: Table02R1.doc

Laboratory code	Location	Depth (m)	De (Gy)	Dose rate (mGy/a)	OSL date BP (ka)
X1598	Glaciolacustrine deposit (Section LB1, Unit 2)	22.5	64 ± 14	1.32 ± 0.06	49 ± 11
X1599	Glaciolacustrine record (Section LB1, Unit 2)	29.5	100 ± 5	1.22 ± 0.06	82 ± 6
X1600	Glaciolacustrine record (Section LB1, Unit 2)	35	75 ± 12	1.36 ± 0.06	55 ± 9
X1601	Kame terrace deposits Moraine of Viu	3	86 ± 13	1.75 ± 0.08	49 ± 8

Table 03

Click here to download Table: Table03R1.doc

PYRENEES AND EBRO BASIN (overall data) (Sites located in Fig. 1B, this work)	**AGE Ka (BP)**	**Marine Isotope Stage (age ka)**	**LINÁS DE BROTO-VIU (this work)** (Figs. 2 and 3, Table 2)	**OSL dates ka (BP)**
		MIS 2		
		29-30		
5-Moraine b, Valira Valley (Andorra)	32			
6-Moraine, Ariège Valley (France)	35		Fragen moraine	
2a-Moraine, Senegüé (River Gállego)	36±3			
		MIS 3	Units 3, 4 and 5 (LB 1)	
2c-Fluvial terrace aggradation (River Gállego)	45±3		Viu moraine (kame terrace)	49±8
4b-Fluvial terrace aggradation (River Cinca, Qt8)	47±4		Unit 2 (LB1)	49±11 55±9
			Unit 1 (LB1)	> 55±9
		60-61		
5-Moraine a, Valira Valley (Andorra)	59±1		MAXIMUM EXTENT OF THE ARA GLACIER	
4c-Terrace Qt7 (River Cinca)	61±4			
4a-Terminal moraine, Salinas de Sin (River Cinca/Cinqueta)	64±11			
2b-Glaciofluvial terraces (River Gállego)	68±7	**MIS 4**		
1b-Moraine, Castiello (River Aragón)	68±7			
1a-Fluvial terrace, Aragón valley (River Aragón)				